Results in Engineering 32 (2026) 113608

Contents lists available at ScienceDirect

Results in Engineering

journal homepage: www.sciencedirect.com/journal/results-in-engineering

Research paper

Base-generated functional groups as active drivers for the enhanced retention of gaseous formaldehyde on microporous carbon

Kowsar Ahmadi, Hubdar Ali Maitlo, Ki-Hyun Kim *

Department of Civil and Environmental Engineering, Hanyang University, 222 Wangsimni-ro, Seongdong-Gu, Seoul, 04763, Republic of Korea

ARTICLE INFO

Keywords:
Adsorption
Activated carbon (AC)
Bases
Formaldehyde (FA)
KOH

ABSTRACT

The applicability of functionalized activated carbon (AC) as an adsorbent for the removal of a polar volatile organic compound, specifically formaldehyde (FA) is investigated. Pristine activated carbon (AC_o) is functionalized with four basic reagents (NH_4OH, NaOH, K_2CO_3, and KOH) and coded as AX-y, where A, X, and y denote the AC support, the reagent (A, N, C, and K, respectively), and the modifier molarity, respectively. The FA adsorption performance of these AX samples is evaluated with respect to key operational parameters. Among all samples, AK-3 exhibits the best performance, achieving the highest breakthrough volume through a synergistic pore-filling physisorption and localized chemisorption. At 0% RH, 10 Pa FA, and 100 mL min^{-1}, AK-3 achieves a 3.3-fold higher capacity (25.52 vs 7.71 mg g^{-1}) and ~3-fold higher partition coefficient (0.085 vs 0.030 mol kg^{-1} Pa^{-1}) than pristine AC_o, despite only a 0.2% increase in micropore surface area (1021 vs 1019 m^2 g^{-1}). Characterization confirms abundant surface functional groups (hydroxyl, carboxylate, and quinone) that enhance chemical adsorption of polar FA. Isotherm-kinetic modeling, together with a low mean adsorption energy (E = 0.225 kJ mol^{-1}), indicates that FA uptake is dominated by physisorption within micropores, while in situ DRIFTS reveals localized surface-assisted chemisorption and oxidation at basic oxygen sites. This work establishes a quantitative structure-surface chemistry-performance relationship, clarifying how specific functional groups modify the nonpolar AC surface and enhance its adsorption of challenging polar VOCs through a dual-mode mechanism combining micropore physisorption with localized surface-assisted chemisorption and oxidation.

1. Introduction

Formaldehyde (FA), a prevalent and highly toxic volatile organic compound (VOC), is recognized as one of the most critical indoor air pollutants. Its emissions originate primarily from building materials, furnishings, and industrial processes [1]. Exposure to FA poses serious health risks, ranging from acute irritation of the eyes, skin, and respiratory tract to chronic conditions such as asthma and an increased risk of cancer [2]. Consequently, significant research has focused on developing effective remediation technologies (e.g., adsorption, reactive adsorption, thermo-catalysis, and photocatalysis) to mitigate FA emission [2,3]. Adsorption is a particularly attractive technology for indoor FA control, as it functions effectively under ambient conditions with low energy demand and simple operation, providing key advantages over catalytic and photocatalytic methods [1,4]. Among adsorbents, activated carbon (AC) holds the greatest industrial promise due to its scalability, low cost, and established pore structure, which facilitate its direct integration into practical air purification systems [5,6].

Despite its advantages, the intrinsically nonpolar surface of pristine AC (AC_o) limits its affinity for polar adsorbates such as FA, constraining its adsorption capacity [7]. This incompatibility arises because the polar carbonyl group (C=O) bond group of FA interacts weakly with the nonpolar AC_o surface [8]. Despite numerous reports of enhanced adsorption after alkaline treatment of activated carbon, the specific origin of the improvement remains insufficiently resolved. In particular, it is difficult to distinguish the contribution of changes in pore structure from that of newly introduced surface functional groups [9]. This distinction is especially important for commercial microporous carbons, for which alkaline treatment may modify surface chemistry without substantially increasing the overall surface area. Moreover, under dynamic gas-phase conditions, the relative contributions of pore-filling physisorption, surface-specific interactions, and possible surface transformations of formaldehyde have not been systematically clarified. Therefore, a structure–surface chemistry–performance relationship is

* Corresponding author.
E-mail address: kkim61@hanyang.ac.kr (K.-H. Kim).

https://doi.org/10.1016/j.rineng.2026.113608
Received 7 August 2026; Received in revised form 5 October 2026; Accepted 14 October 2026
Available online 16 October 2026
2590-1230/© 2026 The Authors. Published by Elsevier B.V. This is an open access article under the CC BY-NC-ND license (http://creativecommons.org/licenses/by-nc-nd/4.0/).

still needed to explain why different alkaline modifiers produce different FA uptake behaviors [10]. Treatment with basic reagents such as ammonium hydroxide (NH_4OH), sodium hydroxide (NaOH), potassium carbonate (K_2CO_3) and potassium hydroxide (KOH) has proven effective in enhancing the adsorption of VOCs, including FA [11–13]. Alkaline modification can influence FA uptake through several potentially overlapping pathways. First, chemical treatment can introduce or enrich polar oxygen-containing functional groups, such as hydroxyl, carboxylate, and quinone groups, on the carbon surface. These groups may act as specific active sites, promoting stronger interactions with polar FA molecules through hydrogen bonding and Lewis acid–base interactions, thereby contributing to surface-specific adsorption [14,15]. Second, alkaline treatment may also modify the porous structure, improving the accessibility of micropores and mesopores and facilitating physisorption through dispersive interactions and pore filling. The resulting pore network also improve access to chemically active surface sites. In addition, these surface functionalities may promote surface transformations of adsorbed FA species. Distinguishing these contributions is important because a material may exhibit predominantly physical adsorption while still showing spectroscopic evidence of surface-specific interactions [16]. The present study therefore considers physisorption, surface chemical interactions, and possible surface reactions as complementary rather than mutually exclusive pathways. However, the literature has yet to clearly establish the relative importance of these contributions under dynamic gas-phase FA adsorption conditions. In particular, it remains unclear whether the enhanced uptake produced by different alkaline modifiers is governed mainly by changes in pore structure, surface chemical functionality, or their combined effects.

To address the ambiguities outlined above, this investigation undertakes a systematic comparison of four widely used alkaline modifiers, NH_4OH, NaOH, K_2CO_3, and KOH, under rigorously controlled conditions to decouple the influence of basic site identity and loading on FA uptake. Rather than assuming that enhanced adsorption results from pore development alone, this study evaluates the adsorption performance in relation to the relatively limited changes in textural properties and the formation of oxygen-containing surface functionalities [1]. While previous studies have examined individual modifiers or equilibrium capacity alone, this work employs an integrated methodology combining breakthrough analysis, thermodynamic partition coefficients, and in situ DRIFTS spectroscopic evidence to assess performance under dynamic flow regimes relevant to real-world application. The novelty of this study lies in the systematic comparison of NH_4OH, NaOH, K_2CO_3, and KOH using the same commercial microporous carbon under dynamic gas-phase FA conditions, with particular emphasis on distinguishing the contribution of surface chemistry from that of the largely preserved porous structure. By combining breakthrough measurements, partition coefficients, physicochemical characterization, humidity-dependent experiments, cyclic operation, and in situ DRIFTS, the study provides an integrated assessment of how base-induced surface chemistry contributes to FA adsorption. Accordingly, the objectives of this study were to: (i) compare the effects of NH_4OH, NaOH, K_2CO_3, and KOH modification on the dynamic adsorption of gaseous FA; (ii) identify the alkaline treatment condition providing the most favorable adsorption performance; (iii) determine whether the observed improvement can be explained primarily by changes in pore structure or by changes in surface chemistry; and (iv) clarify the relative roles of physical adsorption and surface-specific interactions using breakthrough behavior, adsorption models, surface characterization, humidity effects, cyclic operation, and in situ DRIFTS. Based on these objectives, we hypothesize that the enhanced performance of the optimized material is associated primarily with the introduction of oxygen-containing surface functionalities, while the underlying microporous structure remains largely preserved.

2. Materials and methods

2.1. Materials

Granular activated carbon used in this study was obtained from DUKSAN Pure Chemical Co., Ltd. (Ansan, Gyeonggi, South Korea). The AC_o was ground manually using a mortar and pestle, then sieved to isolate particles ranging in size from 212 to 260 μm. paraformaldehyde (PFA, 95%) was purchased from Sigma-Aldrich (St. Louis, MO, USA). Potassium carbonate (K_2CO_3, > 99%) was procured from Tokyo Chemical Industry Co., Ltd. (Tokyo, Japan), while sodium hydroxide (NaOH, 97% purity), ammonium hydroxide (NH_4OH), and potassium hydroxide (KOH, 90%) were all supplied by Sigma-Aldrich (St. Louis, MO, USA). A primary standard (PS) of gaseous FA in nitrogen (N_2) was generated by the thermal depolymerization of paraformaldehyde at 90 °C [17]. The FA primary standard was stored in a polyester-aluminum (PEA) laminate gas sampling bag (Model No. 205–3001–40), which was obtained from Top Trading Co. (Seoul, South Korea).

2.2. Preparation of modified activated carbon

A mass of 1000 mg of AC_o was added to separate 250 mL Pyrex® beakers, each containing 100 mL of an aqueous solution of KOH, NaOH, K_2CO_3, and NH_4OH at a specified molarity (0.1, 2, 3, and 4 M). The mixture was stirred vigorously (300 rpm) at 80 °C for 5 h. After cooling to room temperature, the resulting material was washed five times with deionized water until no further change in pH (neutral pH of 7) could be detected. After filtration, the modified AC samples were dried in a convection oven at 80 °C for 12 h (Fig. 1). The resulting functionalized samples were designated according to the coding scheme in Table 1. The sample coding follows the format AX-y, where A represents the activated carbon base material, X identifies the chemical modifier (A for NH_4OH, N for NaOH, C for K_2CO_3, and K for KOH), and y indicates the molar concentration of the modifier solution. The complete list of sample names is as follows: AC_o, AA-0.1, AA-2, AN-0.1, AN-2, AC-0.1, AC-2, AK-0.1, AK-1, AK-2, AK-3, and AK-4.

2.3. Characterization of modified activated carbon

A range of analytical techniques was used to investigate the physicochemical characteristics of the modified samples, including their crystal structure, elemental composition, surface properties (surface area, pore volume, and average pore diameter), and morphology. Surface functional groups of the modified ACs were analyzed by Fourier transform infrared spectroscopy (FTIR; Nicolet 5700, Thermo Fisher Scientific, USA) in attenuated total reflectance (ATR) mode, scanning from 400 to 4000 cm^{-1}. Powder X-ray diffraction (PXRD; D8 Advance, Bruker, Germany) was used to determine the crystal structure of the samples. Measurements were taken over a 2θ range of 5° to 80° with a step size of 0.02° and a scan rate of 4° min^{-1}. Surface area, pore volume, and pore diameter were evaluated using nitrogen (N_2) adsorption-desorption isotherms, based on the Brunauer-Emmett-Teller (BET: TriStar II, Micromeritics Instrument Corp, USA) method. All samples were degassed at 150 °C for 17 h before measurement. The morphological properties of the samples were assessed by scanning electron microscopy (SEM: Zeiss, Germany). Elemental analysis (EA: FLASH EA1112, Thermo Fisher Scientific, USA) was carried out to determine the nitrogen content and surface elemental composition of the adsorbents. Additionally, surface chemical states were investigated by X-ray photoelectron spectroscopy (XPS: K-Alpha Plus, Thermo Fisher Scientific, USA), with all spectra charge-corrected to the C1s peak at 284.5 eV. Zeta potential was measured on a Malvern Zetasizer Nano ZS at 25 °C, with samples dispersed in deionized water and equilibrated for 120 s prior to each measurement.



Fig. 1. Schematic of the synthesis procedure of AC-KOH (AK), AC—NaOH (AN), AC-K_2CO_3 (AC), and AC—NH_4OH (AA).

Table 1
Detailed information of the adsorbent sample codes developed for the abatement of gaseous FA.

Order	Sample	Sample code(1)	Mass of components (mg)(2)					Molar [M] concentration (3)			
			Activated carbon [A]	NH_4OH [A]	NaOH [N]	K_2CO_3 [C]	KOH [K]	NH_4OH [A]	NaOH [N]	K_2CO_3 [C]	KOH [K]
[A] Activated Carbon Treated with 0.1 M Bases (AX-0.1)											
1	pristine AC	AC_o	1000	-	-	-	-	-	-	-	-
2	AC- NH_4OH	AA-0.1	1000	350.4	-	-	-	0.1	-	-	-
3	AC-NaOH	AN-0.1	1000	-	400.0	-	-	-	0.1	-	-
4	AC- K_2CO_3	AC-0.1	1000	-	-	1382.1	-	-	-	0.1	-
5	AC-KOH	AK-0.1	1000				561.1	-	-	-	0.1
[B] Activated Carbon Treated with 2 M Bases (AX-2)											
6	AC- NH_4OH	AA-2	1000	7008.0	-	-	-	2.0	-	-	-
7	AC-NaOH	AN-2	1000	-	7999.4	-	-	-	2.0	-	-
8	AC- K_2CO_3	AC-2	1000	-	-	27,642.0	-	-	-	2.0	-
9	AC-KOH	AK-2	1000	-	-	-	11,221.2	-	-	-	2.0
[C] Activated Carbon Modified with KOH at varying molar concentration (AK-y)											
10	1 M AC-KOH	AK-1	1000	-	-	-	5610.6	-	-	-	1.0
11	3 M AC-KOH	AK-3	1000	-	-	-	16,831.8	-	-	-	3.0
12	4 M AC-KOH	AK-4	1000	-	-	-	22,442.4	-	-	-	4.0

(1) The two-digit sample code follows the format AX-y, which systematically identifies the support material ('A' for activated carbon), the chemical modifier ('X'), and the molar concentration ('y') used in the surface modification process.
(2) The chemical modifier 'X' in AX has been determined as follows: AC—NaOH as AN (N from NaOH), AC-KOH as AK (K from KOH), AC-K_2CO_3 as AC (C from Carbonate), and AC—NH_4OH as AA (A form Ammonium).
(3) The molar concentration ('y') of the chemical modifier spanned from 0.1 to 4 M for the best-performing adsorbent (AK-y). For all other modifier series, a comparative analysis was conducted at two concentration levels (y) of 0.1 M (low) and 2 M (high), so as to provide a comparative assessment across low and high treatment levels.
Note that the molecular weights of NH_4OH, NaOH, K_2CO_3, and KOH used in this study are 35.04 g/mol,39.997 g/mol, 138.21 g/mol, and 56.106 g/mol, respectively.

2.4. Experimental procedure

2.4.1. FA adsorption experiment

A fixed-bed reactor was prepared by packing 25 mg of a powdered modified sample into a cylindrical quartz tube, secured with quartz wool plugs at both ends. Prior to the adsorption runs, all adsorbent-loaded quartz tubes were thermally conditioned at 150 °C for 1 hour under a continuous nitrogen flow (200 mL min^{-1}) using a CT2000 tube reactor cleaning system (Kemtecins Co. Ltd., Republic of Korea). The FA concentration in the outlet stream was analyzed using a gas chromatography-flame ionization detector system (GC-FID; PRG-2010, Shimadzu, Kyoto, Japan) equipped with a large-volume injection (LVI) autosampler. One end of the quartz reactor was connected to the FA-containing PEA bag, while the opposite end was linked to the LVI/GC-FID system. The adsorption experiments were systematically conducted to evaluate the effects of alkaline modifier concentration, FA partial pressure, relative humidity (RH), gas flow rate, and adsorption cycling. For alkaline modification, 0.1 and 2 M were initially investigated for all modifiers, while additional concentrations of 1, 3, and 4 M were examined for the best-performing base. Each experiment was repeated three times. The FA partial pressure was varied from 5 to 20 Pa (5, 10, 15, and 20 Pa), RH was varied from 0 to 80% (0, 20, 50, and 80%), and the inlet gas flow rate was varied from 50 to 150 mL min^{-1} (50, 100, and 150 mL min^{-1}). For cyclic adsorption tests, three consecutive adsorption cycles were conducted. During the experiment, the LVI module pulled the gas stream through the adsorbent bed at a sampling flow rate of 240 mL min^{-1} for varying time intervals (0.1, 0.5, 1, 2, 5, and 10 min).

2.4.2. Data analysis

The FA breakthrough level for each prepared material was calculated as the ratio of the outlet concentration to the inlet concentration, as expressed in Eq. (1).

$$\frac{C_{out}}{C_{in}} = \frac{(C_{out})_n + (C_{out})_{n-1}}{(2 \cdot C_{in})} \quad (1)$$

The C_{in} denotes the initial concentration of the target FA in the working standard (WS) bag, while C_{out} represents the concentration measured in the outlet stream after FA gas has passed through the adsorbent bed. The subscript n corresponds to the measurement index in the sequence of large-volume injection (LVI) events. The adsorption

capacity (Q: mg g^{-1}) was subsequently determined using the equation provided in Eq. (2).

$$Q = \sum \left[C_{in} - 0.5\left(C_{out,n} + C_{out,\ n-1)}\right)\right] \times \Delta V_n \quad (2)$$

where ΔV_n denotes the volume interval (L).

Because adsorption capacity (Q) is strongly influenced by the initial FA concentration, the partition coefficient (PC; mol kg^{-1} Pa^{-1}) was also calculated (Eq. (3)). This provides a more normalized, less biased metric for evaluating adsorbent performance [18,19].

$$PC = \frac{Q}{p \times M} \quad (3)$$

In Eq. (3), p is the outlet pressure (Pa) of FA in the gas stream, while M represents the molar mass (g mol^{-1}) of the adsorbate. Moreover, to ensure that the quantity of FA retained on the adsorbent remains within the safety limits recommended by environmental and occupational protection authorities, the PC and adsorption capacity at the early breakthrough stage of 10% ($BT_{10\%}$) are considered useful indicators for evaluating the practical performance of adsorbents [20].

2.5. Adsorption studies

2.5.1. Isotherm modeling of adsorption

The adsorption isotherms were analyzed through the Langmuir, Freundlich, Dubinin–Radushkevich (D–R), and Temkin models (Eqs. (4)–7). Because the data were obtained from dynamic fixed-bed breakthrough experiments at different FA partial pressures, these models were used as comparative descriptions of the pressure-dependent adsorption behavior rather than as strict equilibrium isotherms. The Langmuir model describes monolayer adsorption equilibrium on a surface with a finite number of uniform, energetically identical sites [21,22]. At low pressures, it converges toward Henry's law by assuming that adsorption is directly related to the availability of unoccupied surface sites [23]. In contrast, the Freundlich model accounts for multilayer adsorption on heterogeneous surfaces and describes reversible adsorption [24]. The D-R model is an empirical equation used to estimate the mean adsorption energy for a pore-filling mechanism, applicable to both homogeneous and heterogeneous surfaces [21]. Meanwhile, the Temkin model proposes that the heat of adsorption decreases linearly with increasing surface coverage, assuming a uniform distribution of binding energies (BEs) up to a maximum value [25].

$$Q_e = \frac{Q_m K_L\ P}{1 + K_L P} \quad (4)$$

$$Q_e = K_F P^{1/n} \quad (5)$$

$$Q_e = Q_s \exp\left(-K_{ad}\varepsilon^2\right) \quad (6)$$

$$Q_e = B ln(A * P) \quad (7)$$

Here, Q_m and Q_s denote the adsorption capacity at monolayer coverage (mg g^{-1}), while P represents the FA partial pressure (Pa). The constants K_L (Pa^{-1}) and K_F (mg g^{-1} $Pa^{-(1/n)}$) correspond to the Langmuir and Freundlich parameters, respectively, with n indicating the adsorption intensity that reflects the degree of adsorbent–adsorbate interaction. In the D–R model, the constant K–ad (mol^2 kJ^{-2}) theoretically represents the mean adsorption energy, whereas ε is the Polanyi potential (kJ mol^{-1}), defined as $\varepsilon = RT \ln(1 + 1/P)$. For the Temkin model, B is a constant related to the heat of adsorption ($B = RT/b$), where b is the Temkin constant (J mol^{-1}). Here, T is the absolute temperature (K), R is the universal gas constant (8.314 J mol^{-1} K^{-1}), and A denotes the Temkin isotherm constant (mg g^{-1} Pa^{-1}).

2.5.2. Kinetic modeling of adsorption

The adsorption kinetics were evaluated using the pseudo-first-order (PFO), pseudo-second-order (PSO), Elovich, and intraparticle diffusion (IPD) models (Eqs. (8)–11). The Elovich model is typically applied to chemisorption on heterogeneous surfaces, where the activation energy for adsorption varies with surface coverage [26]. In contrast, the IPD model primarily accounts for the influence of the boundary layer during the adsorption process [27].

$$Q_t = Q_s(1 - \exp(-K_1 t)) \quad (8)$$

$$Q_t = \frac{Q_s^2 K_2\ t}{1 + Q_s K_2 t} \quad (9)$$

$$Q_t = \frac{1}{\beta} ln(1 + a\beta t) \quad (10)$$

$$Q_e = K_{ID} t^{0.5} + C \quad (11)$$

Here, Q_t denotes the adsorption capacity at time t, while Q_s refers to the maximum theoretical adsorption capacity (mg g^{-1}). The kinetic rate constants are represented as K_1 (min^{-1}) for the PFO model, K_2 (g mg^{-1} min^{-1}) for the PSO model, and K_{ID} (mg g^{-1} $min^{-0.5}$) for the IPD model. In the Elovich model, α (mg g^{-1} min^{-1}) corresponds to the initial adsorption rate, while β (g mg^{-1}) indicates the surface coverage associated with chemisorption. The constant C (mg g^{-1}) relates to the boundary layer thickness; a larger C value indicates a greater contribution from surface or film diffusion to the overall rate [24].

3. Results and discussion

3.1. Physicochemical characterization of prepared materials

The PXRD patterns of the AK-3 and its counterparts (i.e., AC_o, AA-2, AN-2, AC-2, and AK-2) are shown in Fig. 2. The PXRD analysis indicates that all material possesses the characteristic amorphous structure of activated carbon (Fig. 2). This is evidenced by the two broad reflections corresponding to the (002) plane (related to layer stacking, observed around 2θ of 20° and 26°) and the (100) plane (related to in-plane ordering, observed around 2θ of 42°) (Fig. 2) [24]. The broadness of these peaks indicates a high degree of structural disorder and very small graphitic crystallite sizes [28]. Furthermore, the chemical treatments with various alkaline agents did not induce any significant change in the overall long-range crystalline order, as the peak positions and shapes remain consistent across all samples. This suggests that the modifications primarily affect the surface chemistry and pore structure (e.g., creating new pores or introducing functional groups) rather than transforming the fundamental carbon framework into a more graphitic

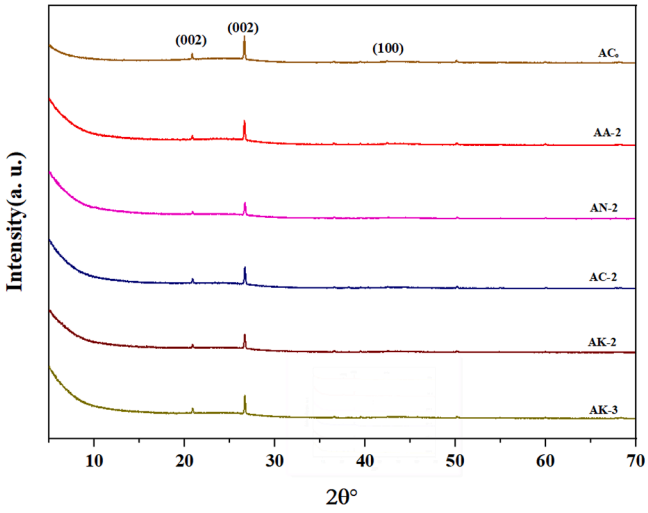

Fig. 2. XRD patterns of all tested AC samples.

state.

Additionally, the crystallite size data, derived from the PXRD analysis, provides crucial insight into the structural order of the materials, which correlates with a more developed pore structure and higher surface area. Compared to other samples, AK-3 maintains a relatively large crystallite size (49.95 nm) while showing only moderate changes in its textural properties after alkaline treatment (Table 2). These defects and expanded micro/mesopores increase the surface area and pore volume, providing more sites for FA adsorption. This highly porous and disordered structure is ideal for FA adsorption, as the small FA molecules can efficiently penetrate and be trapped within the high surface area and narrow micropores. Therefore, its structural properties including its crystallite size and the effects of KOH modification suggest that AK-3 is well-suited to exhibit superior adsorption capacity and efficiency for FA removal compared to the other modified carbons. Notably, the chemical treatments with various alkaline agents did not induce any significant change in the overall long-range crystalline order (Fig. 2), supporting that, modifications primarily affect surface chemistry rather than the carbon framework.

The N_2 adsorption-desorption isotherms and BET analysis indicated that AK-3 possesses textural properties highly conducive to FA adsorption. All materials exhibited type-IV isotherms with H4-type hysteresis loops, which are characteristic of micro-mesoporous activated carbons (Fig. 3 **(a–f))**. In the case of AK-3, a notably higher overall nitrogen uptake was observed, indicating greater accessible pore volume compared with several of the other samples (Fig. 3**f**). The steeper adsorption branch at low relative pressure ($P/P_0 < 0.1$) indicates a large volume of micropores, critical sites for trapping small polar molecules such as FA (Fig. 3**f**). Meanwhile, the hysteresis loop suggests the presence of mesopores, which facilitate rapid diffusion and reduce mass-transfer resistance. Compared with AC_o and other base-treated materials (e.g., AA-2, AN-2, AC-2, and AK-2), AK-3 showed a moderate increase in average pore diameter (Dn = 2 nm) and mesopore volume ($V_{meso} = 0.084\ cm^3\ g^{-1}$), together with a high micropore surface area ($S_{micro} = 1021\ m^2\ g^{-1}$) (Table 2). This represents only a 0.2% increase from AC_o ($1019\ m^2\ g^{-1}$), supporting that textural development is negligible and that surface chemistry is the dominant factor in the observed performance gain. These changes suggest some modification of the micro-mesoporous structure and may improve the accessibility of adsorption sites, rather than indicating extensive pore development. These structural features can support physisorption and improve the accessibility of surface adsorption sites, thereby facilitating interaction with the polar carbonyl group of FA. Thus, the combination of a high surface area, abundant microporosity, and a modified micro-mesoporous structure makes AK-3 well suited for efficient FA adsorption [28,29].

The superior performance of KOH relative to the other alkaline modifiers can be rationalized by three factors. First, K^+ has a smaller hydrated radius and higher mobility than Na^+ or NH_4^+, allowing deeper penetration into the micropore network and more uniform contact with the carbon surface during impregnation. Second, KOH is a stronger base than NH_4OH and K_2CO_3, and its reaction with surface carbon at 80 °C can generate additional oxygen-containing functionalities through controlled oxidation and etching of edge sites, without the severe structural damage that accompanies high-temperature KOH activation. Third, the K^+ cation can intercalate between graphitic layers, weakening interlayer interactions and exposing additional edge sites for functionalization. In contrast, NaOH is less effective at penetrating the micropores, and NH_4OH decomposes during drying, limiting its functionalization efficiency. K_2CO_3 is a weaker base and requires higher temperatures to decompose into reactive species, resulting in fewer oxygen groups under the mild conditions used here. These differences are consistent with the EDX oxygen contents (6.65 wt% for AK-3 vs. lower values for AA-2, AN-2, and AC-2) and with the Zeta potential shift, which is most pronounced for AK-3.

Formaldehyde (HCHO) capture on AK-3 proceeds via a synergistic dual-mode mechanism that bridges bulk microporous physical storage with localized surface chemical reactivity. As evidenced by Dubinin–Radushkevich ($E = 0.225\ kJ\ mol^{-1}$) and kinetic modeling, physical condensation within micropores accounts for the primary volumetric uptake capacity. However, because AK-3 was prepared via mild aqueous KOH treatment at 80 °Cwithout high-temperature thermal activation, its micropore surface area ($S_{micro} = 1021\ m^2\ g^{-1}$) remains essentially unchanged relative to pristine AC_0 ($1019\ m^2\ g^{-1}$). Consequently, the 3.3-fold enhancement in adsorption capacity is governed predominantly by surface oxygen functional groups (6.65 wt.% O via EDX) rather than structural pore expansion. Under ambient air conditions, co-adsorbed O_2 activated at KOH-induced basic sites drives localized surface-assisted oxidation. Time-resolved in situ DRIFTS directly captures this sequential transformation, showing initial HCHO adsorption evolving into dioxymethylene and subsequently surface formate intermediates. Thus, micropore physisorption provides high capacity, while localized chemisorption and surface oxidation dictate site-specific retention affinity and elevated partition coefficients.

The SEM and EDX analyses confirm the enhanced suitability of AK-3 for FA adsorption by revealing favorable changes in both surface morphology and elemental composition (Fig. 4 **(a, b, and c))**. SEM images show that the AC_o has a relatively smooth surface, whereas AK-3 exhibits a highly rough and porous morphology with cavities and interconnected channels [7]. This increased surface roughness and pore development are the macroscopic evidence of the extensive porosity and high surface area that were quantified by the BET analysis, which is critical for providing maximum physical adsorption sites for the small FA molecules. EDX analysis indicates a significant increase in oxygen content (to 6.65 wt.%) on the AK-3 surface (Fig. 4**(c)**. This increase in oxygen indicates the successful introduction of oxygen-containing functional groups (e.g., hydroxyl, carboxyl, and phenolic groups) during the KOH modification process. These polar functional groups are

Table 2
Textural properties and crystallite sizes of the prepared materials.

Order	Materials codes	Surface area ($m^2\ g^{-1}$)			Pore volume ($cm^3\ g^{-1}$)			Average pore diameter (nm)	Crystallite size (nm)
		Total (S_{BET})	External ($S_{external}$)[a)]	Micropore (S_{micro})[a)]	Total (V_{total})	Micropore (V_{micro})[b)]	Mesopore (V_{meso})[b)]	Dn	D[c)]
1	AC_o	1036	17	1019	0.655	0.458	0.067	1.8	51.32
2	AA-2	949	18	931	0.608	0.434	0.069	1.8	45.260
3	AN-2	968	16	952	0.622	0.429	0.074	1.9	41.86
4	AC-2	1006	18	988	0.641	0.432	0.08	1.9	46.61
5	AK-2	980	16	964	0.626	0.413	0.077	1.9	48.92
6	AK-3	1037	16	1021	0.668	0.467	0.084	2	49.95

a) External surface area and micropore surface area were calculated by t-plot.
b) Micropore and mesopore volumes are calculated using the t-plot method for micropores (< 2 nm) and the BJH (Barrett-Joyner-Halenda) method for mesopores (2 - 50 nm), based on the analysis of N_2 adsorption data at different relative pressures.
c) Crystallite size (D) was determined by X-ray diffraction analysis using the Debye-Scherrer equation.

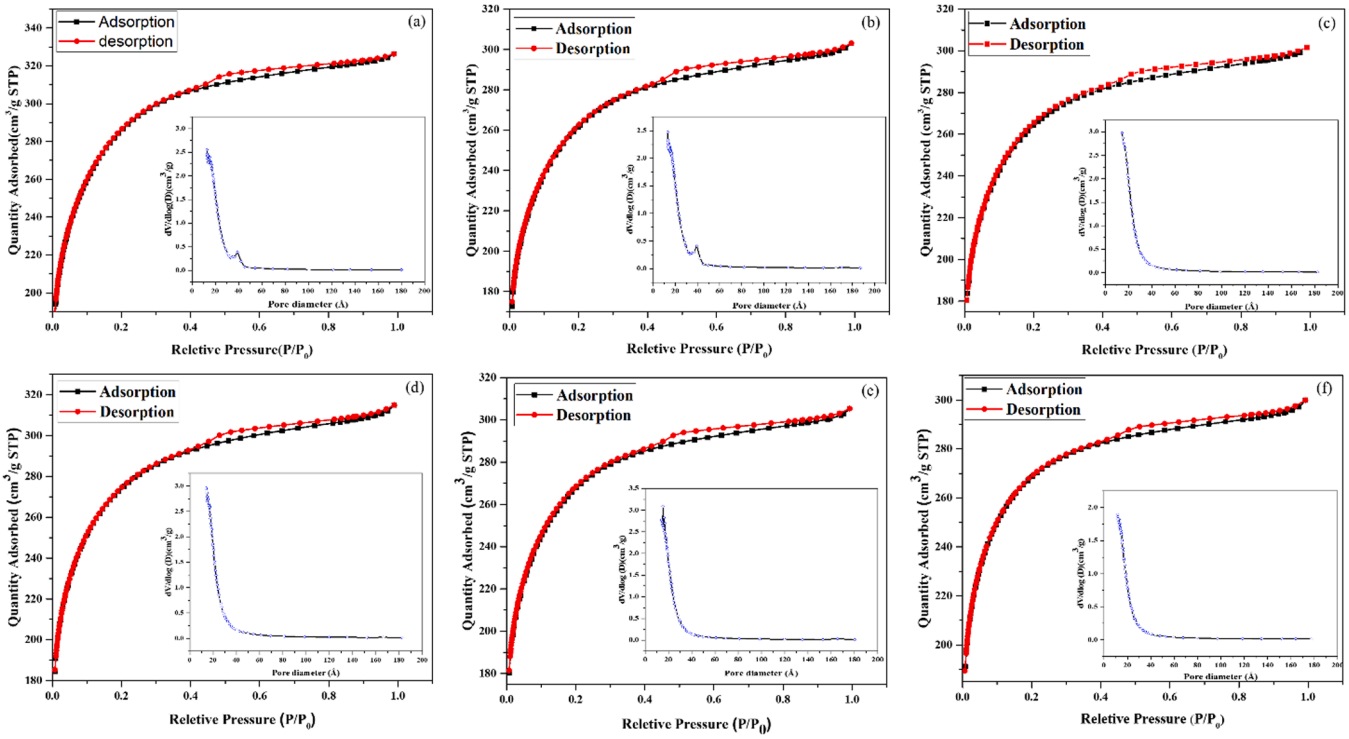

Fig. 3. Nitrogen adsorption-desorption isotherms and BET surface area analysis of the synthesized (a) AC_o, (b) AA-2, (c) AN-2, (d) AC-2, (e) AK-2, and (f) AK-3.

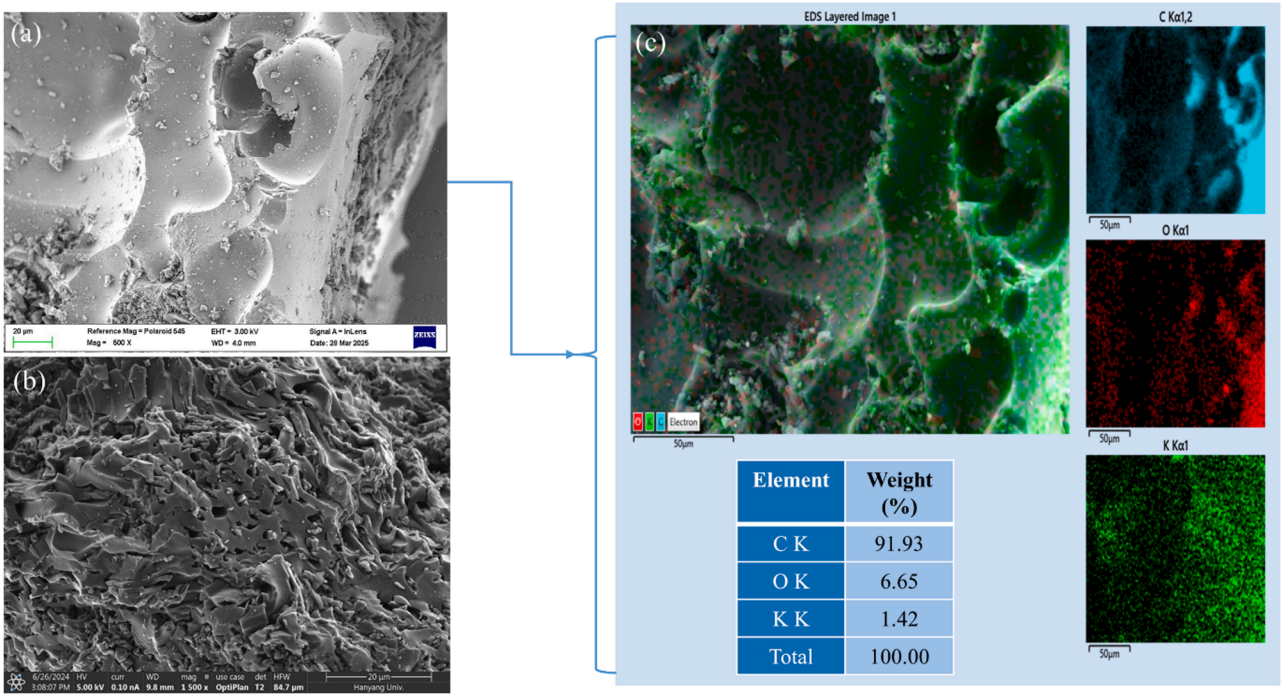

Fig. 4. SEM characterization of adsorbent materials: (a) AK-3, (b) AC_o, and (c) EDX analysis of AK-3 showing C, K, and O wt%.

vital for promoting the chemisorption of the highly polar FA molecule through hydrogen bonding, which significantly enhances adsorption stability and capacity [7]. Consequently, AK-3 offers a powerful synergistic mechanism combining a vast, physically porous structure with a chemically reactive, oxygen-rich surface, making it exceptionally effective for FA removal.

The FTIR analysis indicates the strong potential of AK-3 for FA adsorption by revealing a significant increase in oxygen-containing surface functional groups following KOH treatment (Fig. 5). Specifically, AK-3 displays a clear intensification of key vibrational bands that serve as direct evidence for oxygen group formation: (i) a broad band at 3000–3500 cm^{-1} (O–H stretching of hydroxyl groups), (ii) sharp bands at 1670 and 1750 cm^{-1} (C=O stretching of carbonyl groups), and (iii) a composite band in the 1040–1120 cm^{-1} region (C–O stretching in alcohols, phenols, ethers, and esters) (Fig. 5) [30]. The markedly intensified O–H band directly indicates a higher hydroxyl group density on the AK-3

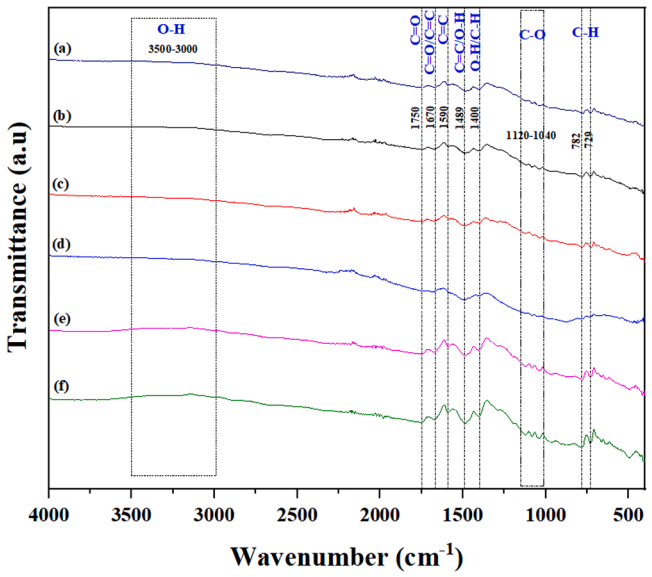

Fig. 5. FTIR functional group identification of all tested AC samples (a) AC_o, (b) AA-2, (c) AN-2, (d) AC-2, (e) AK-2, and (f) AK-3.

surface, which provides abundant active sites for hydrogen-bonding interactions with polar FA molecules, thereby enhancing both physisorption and chemisorption. Concurrently, the strong C–O stretching signals in the 1040–1120 cm^{-1} range corroborate the successful introduction of polar oxygen functionalities that can act as Lewis basic sites, facilitating further surface interactions with FA (Fig. 5) [24]. The presence of these groups is consistent with the proposed synergistic adsorption mechanism (Section 3.6), where surface hydroxyls and carboxylates stabilize FA-derived intermediates such as dioxymethylene and formate.

The XPS analysis of AK-3 provided the definitive chemical evidence for its strong affinity toward FA adsorption by identifying and quantifying the surface functional groups. The C1s spectrum was deconvoluted into graphitic (at 284.5 eV), phenolic/ether (at 285.6 eV), and carbonyl (at 289.2 eV) components (Fig. 6**(b))** [20]. Similarly, the O 1 s spectrum indicates oxygen is present primarily as carbonyl (C=O, ~531.1 eV), hydroxyl/phenolic (C–OH, ~533.1 eV), and ether/adsorbed water (C–O–C/O–H, ~534.7 eV) species (Fig. 6**d**) [20]. The abundant presence of these polar and acidic groups is critical as they serve as active chemical sites for the highly polar FA species. Specifically, the OH and carbonyl groups facilitate strong chemisorption through mechanisms like hydrogen bonding, which ensures the FA is not only captured efficiently but is also firmly retained on the surface. XPS results confirm that KOH modification introduced oxygen-containing functional groups, creating a chemically tailored surface that complements the optimized pore structure of AK-3 for FA adsorption.

Zeta potential measurements were conducted to evaluate the surface charge evolution induced by KOH modification. Both pristine AC_o and AK-3 exhibit negative zeta potential peaks, with distributions centered near −27 mV (AC_o) and −35.4 mV (AK-3), as quantified by the absolute magnitudes in the inset (Fig. 7) [31]. This shift toward a more negative surface potential in AK-3 aligns with XPS and FTIR evidence of KOH-induced oxygen-containing functional groups. The elevated negative charge density provides an electrostatically favorable interface for polar formaldehyde molecules. More specifically, the deprotonated hydroxyl and carboxylate groups (conjugate bases of the O–H and C=O

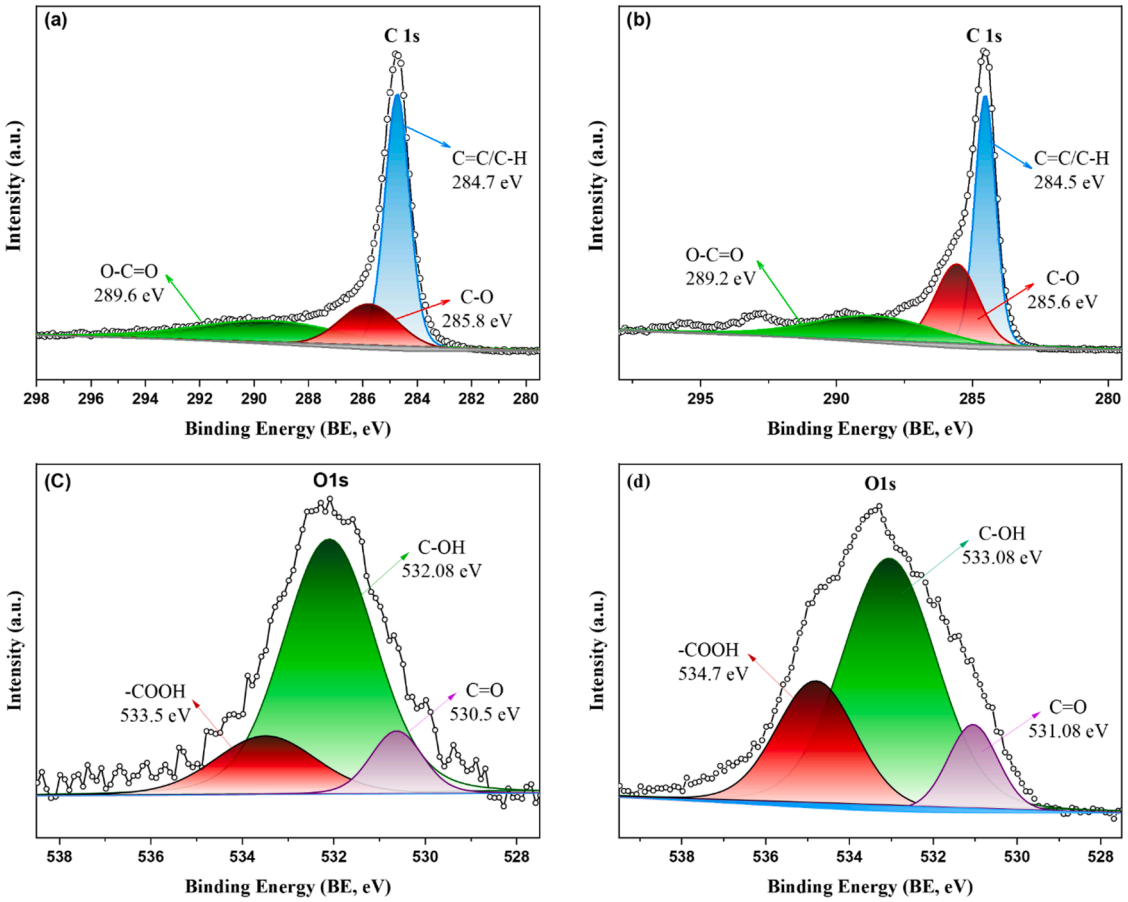

Fig. 6. High-resolution XPS spectra of the adsorbents: C1s for (a) AC_o and (b) AK-3 and O1s for (c) AC_o and (d) AK-3.

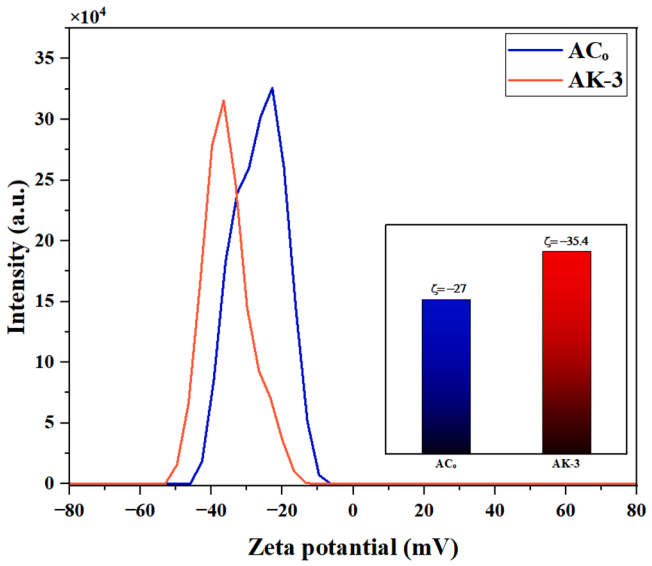

Fig. 7. Zeta potential distribution of AC₀ and AK-3. Inset: average ζ values (−27 mV and −35.4 mV).

functions identified by FTIR and XPS) create electron-rich oxygen sites that can act as nucleophiles toward the electrophilic carbonyl carbon of FA. This nucleophilic addition pathway is consistent with the DRIFTS-observed formation of dioxymethylene and formate intermediates (Section 3.6) and explains why the 0.2% porosity increase alone cannot account for the 3.3-fold capacity enhancement. The Zeta potential shift therefore provides independent electrostatic evidence that KOH modification transforms the carbon surface from a passive physisorbent into a chemically reactive sorbent.

3.2. FA removal performance of prepared adsorbents

FA removal performance was evaluated by measuring dynamic breakthrough at multiple levels (e.g., 10%, 50%, and 100%) to understand adsorption dynamics across the adsorbent's service life. As shown in Fig. 8, the dynamic adsorption performance of the materials was evaluated against 10 Pa FA at dry conditions (0% RH). Their corresponding performance metrics (PC, BTV, and Q values at BT levels of 10, 50, and 100%) are summarized in Table 3. Among all tested materials, AK-3 exhibited significantly improved FA breakthrough behavior. Specifically, the $BTV_{10\%}/BTV_{100\%}$ potential of AK-3 was observed as 74.84/938.2 $L.g^{-1}$, which is approximately 1.1/1.3, 1/1.1, 1.5/1.2, 2.7/2, 2.5/1.2, 3/1.5, 1.4/1.2, 2.8/2.3, 2.6/1.4, 2.3/1.5, 2.6/1.5 times higher than those of AK-4, AK-2, AK-1, AK-0.1, AC-2, AC-0.1, AN-2, AN-0.1, AA-2, AA-0.1, and AC_o adsorbents, respectively (Table 3). Further, the equilibrium Q at 100% BT level (i.e., $Q_{100\%}$: mg g^{-1}) of 10 Pa FA molecules displayed the order of: AK-3 (25.52) > AK-2 (21.75) > AK-4 (18.66) > AN-2 (17.93) > AK-1 (17.86) > AA-2 (14.86) > AA-0.1 (14.02) > AK-0.1 (8.66) > AN-0.1 (7.93) > AC_o (7.71) > AC-0.1 (2.49) (Table 3). Importantly, the PC has also been introduced as a key metric to evaluate adsorbent affinity toward adsorbate molecules [32]. Specifically, the PC at 100% BT level ($PC_{100\%}$ = 0.085 mol·kg^{-1}·Pa^{-1}) value of AK-3 was approximately 1.3, 1.2, 1.4, 3, 2.2, 3.3, 1.4, 3.3, 1.8, 1.8, 2.8 times higher than those of the AK-4, AK-2, AK-1, AK-0.1, AC-2, AC-0.1, AN-2, AN-0.1, AA-2, AA-0.1, and AC_o adsorbents, respectively (Table 3). The superior performance of KOH-activated carbons is attributed to a synergistic mechanism combining physisorption within micropores and chemisorption via basic surface functionalities. Additionally, the enhanced micro- and mesoporosity introduced by KOH modification provides abundant adsorption sites, contributing to the highest FA removal capacity for AK-3. The 3.3-fold enhancement in $Q_{100\%}$ for AK-3 relative to AC₀ was reproducible across triplicate experiments (relative standard deviation <5%), confirming that the improvement is statistically robust and not attributable to experimental variability.

To separate the contribution of increased porosity from that of surface chemical modification, we correlated the micropore surface area (S_{micro}) and total pore volume (V_{total}) from Table 2 with the adsorption capacity ($Q_{100\%}$) and partition coefficient ($PC_{100\%}$) from Table 3 across all samples. The results show that AK-3 exhibits a $Q_{100\%}$ value 3.3 times higher than AC₀, while S_{micro} increases by only 0.2% (1019 to 1021 m^2 g^{-1}). Linear regression of $Q_{100\%}$versus S_{micro} for all 12 samples yields a low correlation coefficient (R^2 < 0.3; n = 12), whereas $Q_{100\%}$ correlates strongly with surface oxygen content (EDX: 6.65 wt.% for AK-3 vs. lower values for other samples). This dramatic improvement driven by surface oxygen enrichment (6.65 wt% O by EDX) rather than porosity directly demonstrates that base-induced functionalization, not pore expansion, governs FA uptake.

3.3. Effect of process variables on AK-3 for fa removal

The operating conditions were established through systematic parameter screening rather than through a formal statistical optimization procedure. The effect of alkaline modifier type and concentration was first evaluated to identify the most effective modified carbon. The selected AK-3 material was subsequently examined under different FA inlet partial pressures, relative humidity levels, and gas flow rates to determine the conditions providing favorable adsorption capacity and breakthrough behavior. Accordingly, the term "optimized" in this study refers to the best-performing condition identified within the experimentally investigated ranges rather than to a statistically optimized global operating condition.

3.3.1. Effect of inlet FA concentration

The effect of FA inlet partial pressure (5–20 Pa) was evaluated at 0% RH and a fixed flow rate of 100 mL min^{-1}. As shown in Table 4 and Fig. 9**a**, increasing FA concentration generally accelerated the breakthrough process, though a non-monotonic trend was observed. The $BTV_{10\%}$ value increased from 66.5 L g^{-1} at 5 Pa to 74.8 L g^{-1} at 10 Pa, followed by a pronounced decrease to 32.3 and 29.8 L g^{-1} at 15 and 20 Pa, indicating rapid saturation of readily accessible adsorption sites under higher concentration gradients (Table 4). Meanwhile, $BTV_{100\%}$ remained relatively stable (857.7–763.2 L g^{-1}), suggesting that total dynamic uptake was largely preserved despite faster early breakthrough at elevated FA levels.

Consistent with this behavior, the Q values increased significantly with FA inlet concentration. The maximum Q ($Q_{100\%}$) rose from 15.48 mg g^{-1} at 5 Pa to 40.11 mg g^{-1} at 20 Pa, reflecting enhanced mass transfer driving force and improved utilization of internal adsorption sites (Table 4). The early-stage Q ($Q_{10\%}$) reached its maximum value of 8.58 mg g^{-1} at 10 Pa and decreased thereafter, indicating that moderate FA concentrations provide an optimal balance between adsorption kinetics and mass transfer zone development. The PC values further support BTV trends. The $PC_{10\%}$ increased markedly from 0.03 to 0.11 mol kg^{-1} Pa^{-1} when the FA partial pressure increased from 5 to 10 Pa, demonstrating strengthened adsorbate–adsorbent interactions during the initial adsorption stage (Table 4). In contrast, $PC_{100\%}$ varied only slightly (0.056–0.085 mol kg^{-1} Pa^{-1}), suggesting that equilibrium adsorption affinity was less sensitive to inlet concentration once the adsorbent approached saturation. Overall, higher FA partial pressures enhance total uptake but shorten the effective mass transfer zone, leading to earlier breakthrough due to accelerated occupation of high-energy adsorption sites [33].

3.3.2. Effect of relative humidity (RH)

The impact of moisture on FA adsorption was evaluated across RH levels of 0–80% at FA = 10 Pa and 100 mL min^{-1} (Fig. 9**b** and Table 4). Water vapor exhibited a strong inhibitory effect, with $BTV_{10\%}$ decreasing from 74.8 L g^{-1} (dry conditions) to 33.3 L g^{-1} (80% RH). The

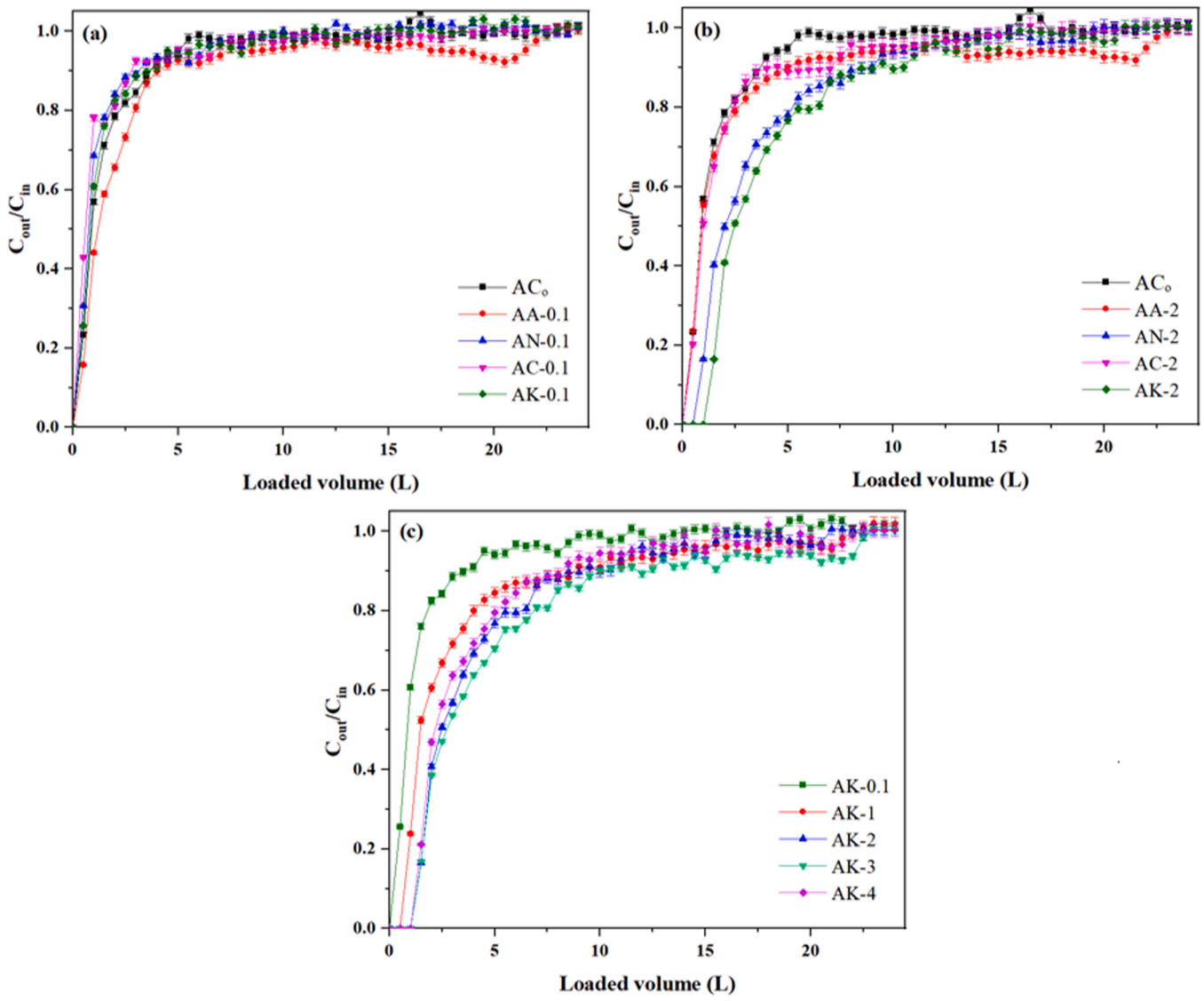

Fig. 8. The breakthrough curves for FA (10 Pa) adsorption onto: (a) 0.1 M base-treated AC samples (AA, AN, AC, and AK) relative to AC_o, (b) 2 M base-modified AC, and (C) breakthrough performances of AC samples treated with different KOH ratios (0.1, 1, 2, 3, and 4 M).

Table 3
Summary of FA adsorption performance for activated carbon modified with different bases.

Order	Material	Breakthrough volume (L g^{-1})			Adsorption capacity (mg·g^{-1})			Partition coefficient (mol·kg^{-1}·Pa^{-1})		
		$BTV_{10\%}$	$BTV_{50\%}$	$BTV_{100\%}$	$Q_{10\%}$	$Q_{50\%}$	$Q_{100\%}$	$PC_{10\%}$	$PC_{50\%}$	$PC_{100\%}$
1	AC_o	29	55.90	643.0	3.402	4.44	7.71	0.041	0.038	0.030
2	AA-0.1	32.66	67.94	633.3	3.83	6.41	14.02	0.060	0.042	0.046
3	AA-2	28.48	56.52	658.5	3.37	5.42	14.86	0.026	0.037	0.048
4	AN-0.1	26.52	50.20	416.6	3.07	4.64	7.93	0.015	0.025	0.026
5	AN-2	52.10	100.32	805.8	6.02	9.47	17.93	0.085	0.064	0.061
6	AC-0.1	24.66	44.00	617.0	2.70	3.85	2.49	0.007	0.028	0.026
7	AC-2	29.84	59.55	768.8	3.47	5.67	11.92	0.036	0.038	0.039
8	AK-0.1	27.80	53.86	475.2	3.21	5.01	8.66	0.022	0.037	0.028
9	AK-2	72.11	118.48	857.0	8.51	9.57	21.75	0.109	0.080	0.071
10	AK-1	48.38	78.31	806.2	5.74	7.92	17.86	0.033	0.054	0.059
11	AK-3	74.84	128.75	938.2	8.58	12.72	25.52	0.110	0.085	0.085
12	AK-4	69.42	106.46	729.7	8.11	10.72	18.66	0.069	0.073	0.063

corresponding early-stage $Q_{10\%}/PC_{10\%}$ declined from 8.58 mg g^{-1}/ 0.11 mol kg^{-1} Pa^{-1} to 3.65 mg g^{-1}/0.07 mol kg^{-1} Pa^{-1}, indicating substantial competition for polar adsorption sites during the initial adsorption phase (Table 4) [34]. This competitive behavior is consistent with Zeta potential measurements (Section 3.1), which show AK-3 carries a more negative surface charge (−35.4 mV) than pristine AC_o (−27 mV); the higher density of polar oxygen groups that produces this charge also increases hydrophilicity, explaining why moisture competes more aggressively for initial adsorption sites.

In contrast, $Q_{100\%}$ showed only a moderate reduction (25.52 to

Table 4
Summary of FA adsorption performance of AK-3 under different experimental conditions.

Order	FA inlet partial pressure Pa	Adsorbent mass (mg)	RH (%)	Flow rate (mL/min)	Reproducibility	Breakthrough volume (L g^{-1})		Adsorption capacity (mg·g^{-1})		Partition coefficient (mol·kg^{-1}·Pa^{-1})	
						$BTV_{10\%}$	$BTV_{100\%}$	$Q_{10\%}$	$Q_{100\%}$	$PC_{10\%}$	$PC_{100\%}$
1	5	25	0	100	-	66.5	857.7	3.79	15.48	0.03	0.066
2	10					74.8	938.2	8.58	25.52	0.11	0.085
3	15					32.3	841.7	5.77	33.00	0.06	0.079
4	20					29.8	763.2	6.87	40.11	0.04	0.056
5	10		0	100	-	74.8	938.2	8.58	25.52	0.11	0.085
6			20			32.5	833.3	3.78	22.93	0.06	0.073
7			50			32.3	878.8	3.60	22.75	0.06	0.095
8			80			33.3	858.0	3.65	22.66	0.07	0.080
9	10		0	50	-	34.4	989.4	4.01	31.51	0.08	0.114
10				100		74.8	938.2	8.58	25.52	0.11	0.085
11				150		30.7	816.2	3.47	15.97	0.04	0.102
12	10	25	0	100	Cycle 1	74.8	938.2	8.58	25.52	0.11	0.085
13					Cycle 2	52.72	917	6.13	17.96	0.094	0.061
14					Cycle 3	30.83	771	3.44	16.63	0.044	0.057

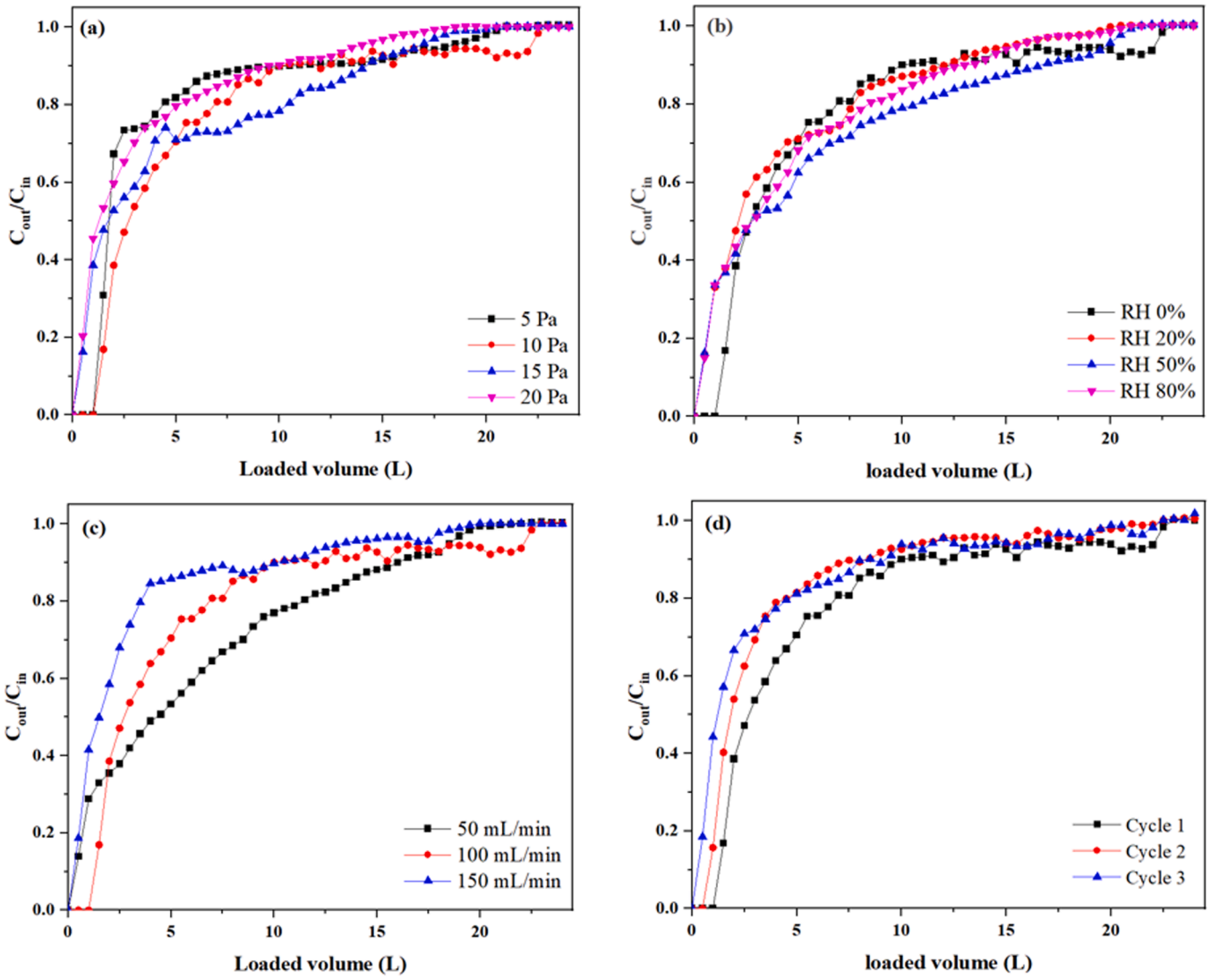

Fig. 9. Adsorption behavior of AK-3: (a) effect of partial pressure, (b) effect of relative humidity, (c) effect of different flow rates, and (d) reusability of AK-3.

22.66 mg g^{-1}), and $PC_{100\%}$ varied slightly (0.085 to 0.08 mol kg^{-1} Pa^{-1}), suggesting that while specific high-affinity sites are preferentially blocked by water molecules, some pore volume remains accessible at saturation. This competitive inhibition can be attributed to the formation of water clusters on the hydrophilic surfaces of AK-3, which physically block pore access and reduce the effective surface area available

for FA capture through hydrogen bonding competition [35]. The minimal effect of relative humidity on $Q_{100\%}$ suggests that FA adsorption at later stages is governed primarily by physisorption within micropores that stay partially accessible under wet conditions. Crucially, even at 80% RH, AK-3 retains 22.66 mg g^{-1} capacity still exceeding the dry-condition performance of many reported sorbents (Table 8). This supports that the material maintains practical utility under realistic indoor humidity. This could be achieved through controlled base loading, post-treatment to remove hydrophilic oxygen groups, or incorporating mildly hydrophobic domains that suppress water clustering without blocking active sites. These strategies, previously shown to enhance VOC selectivity under humid conditions, offer promising routes for optimizing base-modified activated carbon systems.

3.3.3. Effect of inlet flow rate

The influence of inlet flow rate (50 to 150 mL min^{-1}) on FA adsorption was evaluated at a fixed FA partial pressure of 10 Pa and RH = 0% (Fig. 9**c** and Table 4). Increasing the flow rate resulted in progressively earlier breakthrough, as evidenced by a reduction in $BTV_{100\%}$ (989.4 L g^{-1} at 50 mL min^{-1} to 816.2 L g^{-1} at 150 mL min^{-1}), which can be attributed to shortened gas–solid contact time and incomplete utilization of adsorption sites under high space velocity (Table 4). Correspondingly, the $Q_{100\%}/PC_{100\%}$ decreased from 31.51 mg g^{-1}/0.114 mol kg^{-1} Pa^{-1} to 15.97 mg g^{-1}/0.102 mol kg^{-1} Pa^{-1}, indicating that mass transfer limitations become more pronounced at higher gas velocities (Table 4). This behavior demonstrates that insufficient residence time at higher flow rates limits both external mass transfer and intraparticle diffusion, preventing complete utilization of the adsorbent's capacity [36]. External film resistance decreases with increasing flow rate, but reduced contact time dominates the overall adsorption efficiency, resulting in premature breakthrough and lower capacity utilization.

3.3.4. Reproducibility of FA adsorption

Reproducibility tests were conducted to evaluate the operational stability of AK-3 during repeated adsorption cycles. As shown in Fig. 9**d** and Table 4, progressive performance deterioration was observed with successive runs. $BTV_{10\%}$ decreased from 74.8 L g^{-1} in the first cycle to 52.72 L g^{-1} and 30.83 L g^{-1} in the second and third cycles, respectively, while $BTV_{100\%}$ declined from 938.2 to 771 L g^{-1} (Table 4). Similarly, $Q_{10\%}$ decreased from 8.58 to 3.44 mg g^{-1} and $Q_{100\%}$ from 25.52 to 16.63 mg g^{-1} over three cycles (Table 4). The corresponding reduction in $PC_{10\%}$ and $PC_{100\%}$ indicates a gradual weakening of effective FA adsorbent interactions, likely caused by incomplete regeneration, pore blockage by strongly adsorbed FA species, and/or structural fatigue [37]. The observed capacity loss over consecutive adsorption-desorption cycles indicates that a fraction of active sites becomes irreversibly occupied or degraded during FA uptake and subsequent regeneration. This highlights the need for developing optimized regeneration protocols to restore surface functionality. Nevertheless, the initial adsorption capacity of AK-3 (25.52 mg g^{-1}) is comparable to or higher than those of many advanced sorbents reported in the literature, confirming its intrinsic effectiveness under dynamic flow conditions. While the material may require periodic replacement or regeneration after several cycles, its high initial performance supports its potential for practical indoor air purification, especially in scenarios where sorbent replacement is feasible. The practical applicability of AK-3 is further bolstered by the use of KOH, a widely available industrial reagent, and a straightforward modification procedure (aqueous stirring at 80 °C followed by oven drying). While cyclic capacity decay highlights the need for optimized regeneration, AK-3′s initial capacity (25.52 mg g^{-1}) surpasses most literature sorbents (Table 8). Combined with low-cost KOH modification and straightforward synthesis, periodic sorbent replacement remains economically viable for indoor air applications.

3.4. Adsorption isotherm modeling for FA removal

The adsorption equilibrium of gaseous FA on AK-3 was analyzed using Langmuir, Freundlich, Temkin, and Dubinin–Radushkevich (D–R) isotherm models over FA partial pressures of 5–20 Pa (Fig. 10), with the fitting parameters summarized in Table 5. Model validity was evaluated using correlation coefficients (R^2) and chi-square (χ^2) statistics [7].

The Freundlich isotherm provided the best fit to the experimental data ($R^2 = 0.999$ and $\chi^2 = 0.087$), indicating a heterogeneous adsorption surface and a multilayer adsorption mechanism (Table 5). The Freundlich exponent (n = 1.43) Suggesting favorable FA uptake, particularly at elevated inlet partial pressures. This behavior is consistent with the breakthrough curves, where rapid initial FA capture is followed by earlier saturation as high-energy adsorption sites become progressively occupied under continuous flow [38]. The Langmuir model also showed a good correlation ($R^2 = 0.998$ and $\chi^2 = 0.207$), yielding a monolayer adsorption capacity (Q_m) of 93.46 mg g^{-1} and a Langmuir affinity constant (K_L) of 0.036 Pa^{-1} (Table 5). However, the slightly inferior fit compared to the Freundlich model suggests that FA adsorption on AK-3 cannot be adequately described by monolayer coverage on energetically uniform sites, especially under dynamic adsorption conditions [7].

The Temkin isotherm, which accounts for adsorbate-adsorbent interactions and a linear decrease in adsorption heat with increasing surface coverage, resulted in a moderate fit ($R^2 = 0.980$ and $\chi^2 = 2.40$) (Table 5). The Temkin constants (A = 0.440 mg g^{-1} Pa^{-1}; B = 17.75) imply progressively weaker FA-surface interactions at higher surface coverage, providing a mechanistic explanation for the gradual reduction in adsorption efficiency observed in the later stages of the breakthrough curves [33]. The D-R model showed the poorest agreement with the experimental data ($R^2 = 0.904$ and $\chi^2 = 4.889$). The mean adsorption energy (E = 0.225 kJ mol^{-1}) is far below the typical threshold for chemisorption (≈8–40 kJ mol^{-1}), confirming that the majority of FA uptake is governed by physisorption. However, this does not preclude localized chemisorption at a limited number of high-energy basic sites, as evidenced by in situ DRIFTS detection of formate species. The low overall E value reflects that physisorption within micropores dominates the total uptake, while chemisorption contributes to enhanced affinity and retention at specific surface sites, as reflected in the high partition coefficient of AK-3 [7].

Overall, the combined isotherm analysis demonstrates that FA adsorption on AK-3 proceeds via heterogeneous, multilayer, and physisorption-dominated mechanisms with coverage-dependent interaction energies, in excellent agreement with the observed breakthrough

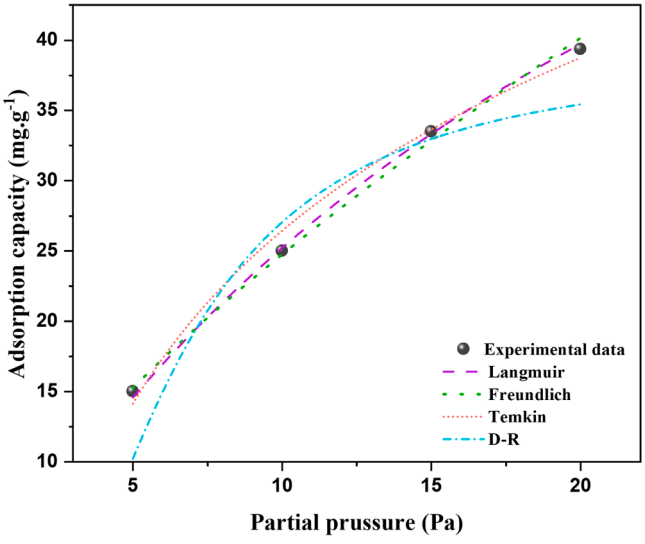

Fig. 10. Adsorption isotherm plots showing the equilibrium uptake of FA on AK-3 with corresponding model fits.

Table 5
Adsorption isotherm parameters of AK-3 derived from different models (Langmuir, Freundlich, D-R, and Temkin).

Order	Model	Parameters	FA
1	Langmuir	Q_m (mg g^{-1})	93.460
		K_L (Pa^{-1})	0.036
		R^2	0.998
		χ^2	0.207
2	Freundlich	K_F (mg $g^{-1}Pa^{-(1/n)}$)	4.961
		n	1.432
		R^2	0.999
		χ^2	0.087
3	Temkin	A (mg $g^{-1}Pa^{-1}$)	0.440
		B	17.750
		R^2	0.980
		χ^2	2.400
4	D-R	Q_t (mg g^{-1})	39.000
		K_{ad} (mol^2 J^{-2})	9.90E-06
		R^2	0.904
		χ^2	4.889
		E (kJ/mol)	0.225

Note: Q (mg g^{-1}) is the experimental equilibrium adsorption capacity at FA partial pressure P (Pa). q_m (mg g^{-1}) refers to the maximum adsorbate mass adsorbed per unit weight. K_L (1/Pa) is Langmuir model constant. K_f and n are Freundlich constants. K_d is the D-R model constant (mol^2/kJ^2). E (kJ/mol) ($=0.001/(2*K_{ad})^{0.5}$): is the free energy representing adsorption types.

and cyclic stability behavior.

3.5. Adsorption kinetic modeling for FA removal

The adsorption kinetics of FA on AK-3 were evaluated using PFO, PSO, Elovich, and IPD models under varying relative humidity (RH = 0–80%) and inlet FA vapor pressures (5–15 Pa) (Figs. 11 and 12 and Table 6). For the experiments at varying RH levels, both the PFO and PSO models provided excellent fits across all RH levels, with consistently high correlation coefficients (R^2 of 0.999), indicating reliable kinetic descriptions. However, the PFO model yielded theoretical adsorption capacities (Qs of 22.6 mg g^{-1} and 21.9 mg g^{-1}) closer to the experimental adsorption capacities (Qe of 22 mg g^{-1} and 21 mg g^{-1}) values, particularly at 0–20% RH, suggesting that FA uptake is predominantly governed by physisorption-controlled surface processes (Table 6) [38]. The gradual decrease in the PFO rate constant (k_1 from 0.025 to 0.014 s^{-1}) with increasing RH (from 0 to 80%) reflects competitive adsorption of water vapor, which slows FA mass transfer without drastically reducing capacity (Table 6). In contrast, the PSO model significantly overestimated Qs (40 mg g^{-1}), especially at 50% RH, implying that chemisorption is not the sole rate-limiting step [39]. The Elovich model also showed good agreement ($R^2 \sim 0.999$), supporting adsorption on energetically heterogeneous surfaces, with decreasing α (0.112 to 0.093 mg g^{-1} sec^{-1}) and β (from 0.853 to 0.551 g mg^{-1}) values at higher RH (from 0 to 80%), further evidencing moisture-induced site blockage [33]. IPD analysis revealed multilinear behavior, indicating that FA adsorption proceeds through multiple steps involving external mass transfer followed by intraparticle diffusion, with neither step solely controlling the overall rate. Overall, the kinetic results demonstrate fast FA adsorption dominated by surface-controlled processes, with humidity primarily affecting diffusion and adsorption rates rather than equilibrium uptake [37].

For the experiments at varying FA inlet pressures, all kinetic models exhibited a high goodness of fit ($R^2 \sim 0.99$), confirming the robustness of the kinetic analysis. The PFO model predicted Qs (i.e., 12.6 mg g^{-1} and 22.6 mg g^{-1}) closely matching the experimental Qe (i.e., 12 mg g^{-1} and 22 mg g^{-1}) values, particularly at 5 and 10 Pa, indicating that FA uptake is primarily governed by surface-controlled physisorption (Table 6) [40]. Although the PSO model provided excellent statistical fits, it substantially overestimated Qs (i.e., Qs of 30.2/51.3/48.1 mg g^{-1} and Qe of 22/33/35 mg g^{-1}) at higher inlet Pa (i.e., 10/15/20 Pa), implying that chemisorption is not the dominant rate-limiting step (Table 6) [39]. The Elovich model also described the data well, reflecting adsorption on energetically heterogeneous surfaces, with decreasing α at higher concentrations indicating progressive site saturation. IPD analysis revealed multilinear behavior, confirming that FA adsorption proceeds through multiple sequential steps involving external diffusion and intraparticle diffusion, with increasing K_{ID1} values at higher inlet FA partial pressures reflecting enhanced concentration-driven mass transfer rather than sole diffusion control [33].

3.6. FA adsorption mechanism of prepared sorbents

To elucidate the surface interactions and reaction mechanisms of FA during adsorption, in situ DRIFTS measurements were performed on AC_o and AK-3 under an air atmosphere (Fig. 13). For AC_o, weak and broad bands appeared across the spectrum, suggesting limited surface

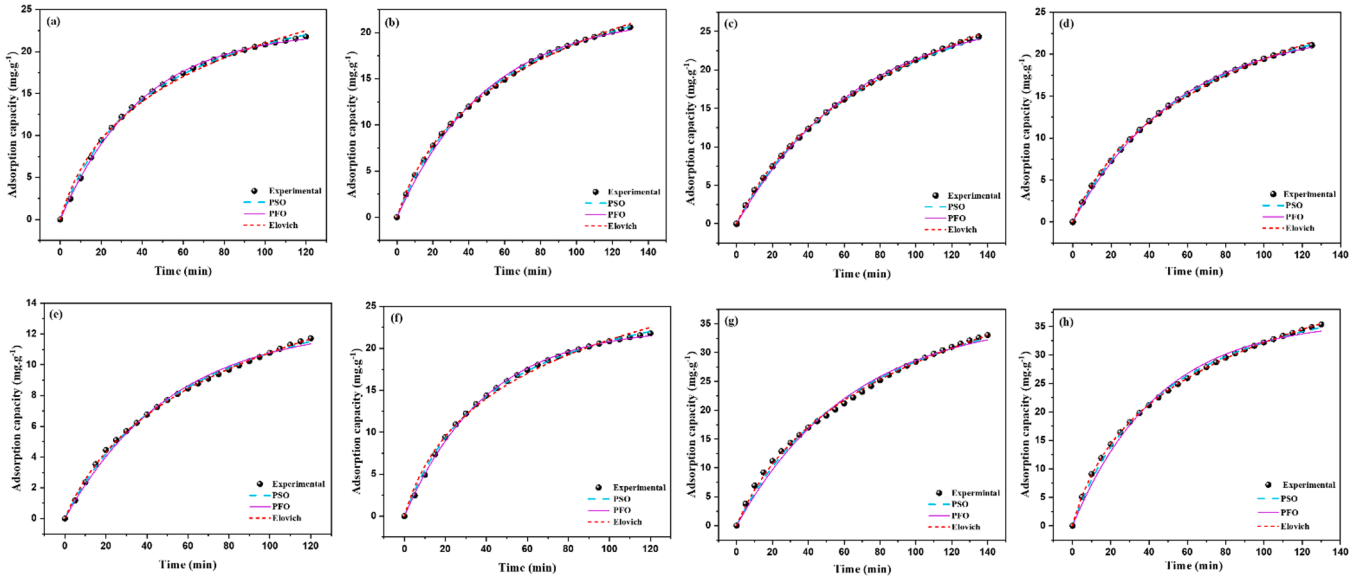

Fig. 11. Non-linear fitting of the pseudo-first-order, pseudo-second-order, intraparticle diffusion, and Elovich models describing FA adsorption under different conditions: (a-d) relative humidity levels (0, 20, 50, and 80%) and (e-h) varying inlet FA partial pressures (5, 10, 15, and 20 Pa).

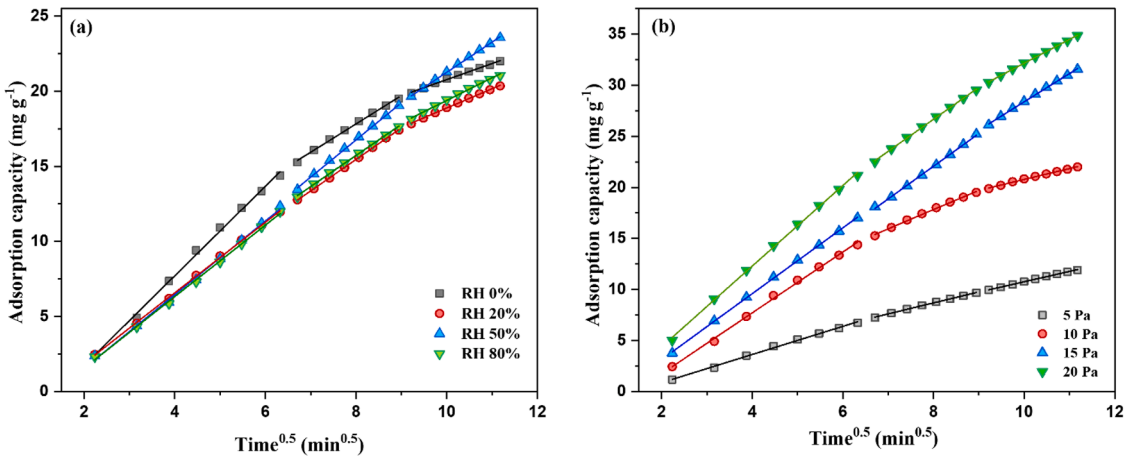

Fig. 12. IPD kinetic modeling for FA adsorption onto AK-3 under varying conditions: (a) Relative humidity (RH, 0–80%) and (b) FA partial pressure (5–20 Pa).

Table 6
Adsorption kinetic parameters of FA onto AK-3 derived from different models (PFOM, PSOM, Elovich, and IPD) under varying relative humidity and concentration conditions.

Order	Kinetic models	Parameters	Relative humidity				Concentration			
			RH 0%	RH 20%	RH 50%	RH 80%	5 pa	10 pa	15 pa	20 pa
Experimental Q_e (mg g^{-1})*			22.0	21.0	24.0	21.0	12.0	22.0	33.0	35.0
1	PFO	Theoretical Q_s (mg g^{-1})	22.6	21.9	27.8	23.2	12.6	22.6	36.4	36.1
		k_1 (sec^{-1})	0.025	0.019	0.015	0.014	0.019	0.025	0.015	0.022
		R^2	0.999	0.999	0.999	0.999	0.996	0.999	0.992	0.992
		χ^2	0.036	0.080	0.050	0.036	0.046	0.036	0.674	0.685
2	PSO	Theoretical Q_s (mg g^{-1})	30.2	30.1	40.0	32.9	17.7	30.2	51.3	48.1
		k_2 (g mg^{-1} sec^{-1})	0.0007	0.0005	0.0002	0.0004	0.0009	0.0007	0.0004	0.0004
		R^2	0.999	0.999	0.999	0.999	0.999	0.999	0.996	0.999
		χ^2	0.046	0.016	0.038	0.003	0.014	0.046	0.337	0.158
4	Elovich	α (mg g^{-1} sec^{-1})	0.112	0.107	0.073	0.093	0.176	0.112	0.060	0.071
		β (g mg^{-1})	0.853	0.615	0.509	0.551	0.323	0.853	0.751	1.250
		R^2	0.994	0.999	0.999	0.999	0.999	0.994	0.999	1.000
		χ^2	0.220	0.035	0.010	0.033	0.006	0.220	0.124	0.008
3	IPD	K_{ID1} (mg g^{-1} $sec^{-0.5}$)	2.98	2.35	2.45	2.38	1.38	2.98	3.22	3.95
		C_{ID1}	−4.210	−2.808	−3.353	−3.180	−1.874	−4.210	−3.300	−3.508
		R^2	0.997	0.999	0.998	0.998	0.997	0.997	0.999	0.999
		χ^2	0.314	0.033	0.176	0.122	0.069	0.314	0.047	0.238
		K_{ID2} (mg g^{-1} $sec^{-0.5}$)	1.89	2.09	2.47	2.07	1.08	1.89	3.17	3.13
		C_{ID2}	2.74	−1.29	−3.03	−0.81	0.09	2.74	−3.49	1.59
		R^2	0.997	0.999	0.999	0.999	0.998	0.997	0.999	0.999
		χ^2	0.044	0.003	0.025	0.017	0.008	0.044	0.055	0.031
		K_{ID3} (mg g^{-1} $sec^{-0.5}$)	1.07	1.29	2.01	1.50	1.01	1.07	2.77	2.33
		C_{ID3}	10.09	5.99	1.18	4.37	0.64	10.09	0.76	8.85
		R^2	0.996	0.999	0.999	0.996	0.998	0.996	0.999	0.999
		χ^2	0.015	0.007	0.009	0.032	0.005	0.015	0.028	0.010

* = The experimental Qe was determined at a reaction time of 120 min, using the same dataset employed for model computation.

reactivity toward FA (Fig. 13**a**). A faint shoulder at 3655 cm^{-1} can be attributed to surface O–H stretching, while very weak absorptions at 1180–1017 cm^{-1} and around 800 cm^{-1} indicate the presence of minor C=O, C–O, and C–H vibrations of adsorbed FA molecules (Fig. 13**(a))** [38]. The absence of identifiable reaction intermediates indicates that FA molecules are only weakly retained within the carbon pores, corresponding to reversible physisorption dominated by dispersive interactions rather than specific chemical bonding. The lack of strong peaks associated with oxidation intermediates implies that FA adsorption on unmodified AC_o is primarily physical, governed by van der Waals interactions with the carbon surface, with negligible chemical transformation [41]. In contrast, the AK-3 spectrum (Fig. 13**b)** displays several well-defined peaks that confirm active surface reactions during FA adsorption [42]. The distinct band at 3655 cm^{-1} corresponds to surface O–H stretching vibrations, whose intensity increases over time, indicating the formation of hydroxylated intermediates [43]. The growth of this band suggests that surface basic sites generated during KOH modification promote nucleophilic addition of FA to hydroxylated carbon sites, forming surface-bound hemiacetal-type species. The bands at 1180 cm^{-1} and 1017 cm^{-1} are characteristic of C=O and C–O stretching in dioxymethylene (DOM) species. The formation of DOM is attributed to the strong chemisorption of FA. This step represents the transition from physisorption to chemisorption, where FA reacts with surface oxygenated/basic groups instead of merely occupying pore volume.

Additionally, strong bands at 1580 and 1356 cm^{-1} are assigned to the asymmetric and symmetric stretching of formate ions ($HCOO^-$), an intermediate product generated from the further oxidation of DOM (Table 7) [44]. The appearance of formate species at 1580 and 1356 cm^{-1} indicates that adsorbed FA undergoes surface-assisted oxidation rather than simple physisorption on AK-3. Importantly, the in situ DRIFTS experiments were conducted under an air atmosphere, providing a continuous supply of molecular oxygen (O_2). The oxidation of DOM to formate is therefore primarily driven by O_2 from the air

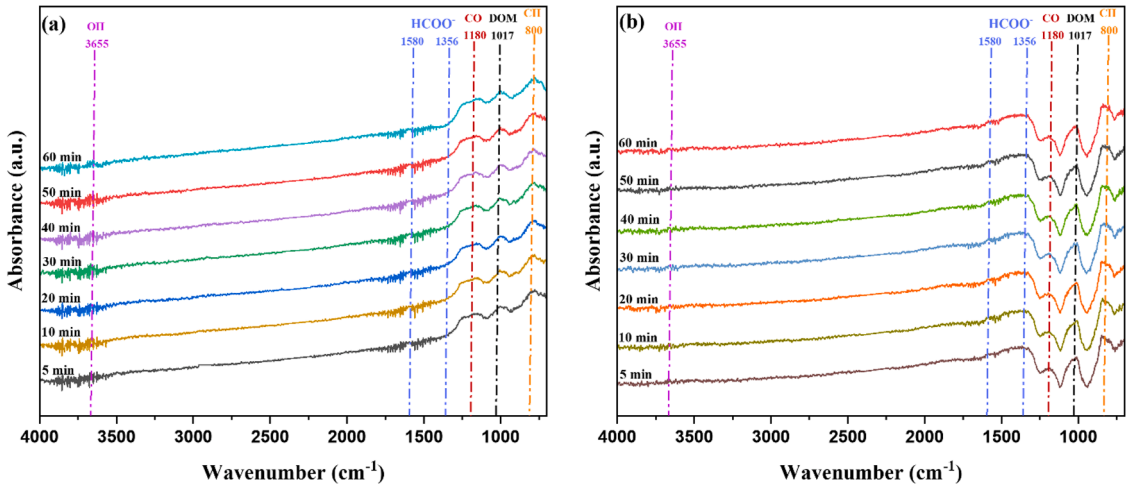

Fig. 13. Time-resolved in situ DRIFTS spectra tracking the evolution of surface species upon FA exposure measured under air atmosphere: (a) AC_o and (b) AK-3.

Table 7
In situ DRIFTS band assignments and proposed surface species during FA adsorption on AC_o and AK-3.

Order	Wavenumber (cm^{-1})	Assignment	Characteristic of	References
1	800	υ(C − H) vibration	C–H vibration of adsorbed FA species	[38]
2	1017	υ(C − O) stretching vibration	C–O stretching associated with dioxymethylene (DOM) species	[44]
3	1180	υ(C = O) stretching vibrations	C=O stretching associated with dioxymethylene (DOM) species	[44]
4	1356, 1580	υ(COO^-) stretching vibrations	Symmetric stretching of surface formate ($HCOO^-$) species	[44]
5	3655	stretching vibrations of υ(OH)	Surface hydroxyl groups and hydroxylated intermediates	[38]

stream. The surface basic sites introduced by KOH treatment (hydroxyl, carboxylate, quinone-like structures) likely assist this oxidation by activating O_2 or stabilizing reactive intermediates, demonstrating intrinsic catalytic activity for FA oxidation mediated by surface oxygenated functional groups. Key band assignments supporting this mechanism include: 3655 cm^{-1} (surface O–H), 1580 cm^{-1} (asymmetric stretching of formate $HCOO^-$), 1356 cm^{-1} (symmetric stretching of formate), and 1180 and 1017 cm^{-1} (C=O and C–O stretching in DOM). We acknowledge that the evidence for FA conversion to formate is indirect, based on DRIFTS peak assignments; while the band positions are characteristic of formate, definitive proof would require isotopic labeling or product desorption analysis in future studies. This surface-assisted oxidation, facilitated by O_2 from air and basic surface sites, contributes to the enhanced retention of FA on AK-3. In summary, FA adsorption on AK-3 follows a dual-mode pathway: (i) bulk physisorption within micropores (E = 0.225 kJ mol^{-1}, Freundlich n = 1.432); and (ii) localized chemisorption at KOH-induced basic oxygen sites, where O_2 from air drives FA conversion to dioxymethylene (1180, 1017 cm^{-1}) and surface formate (1580, 1356 cm^{-1}). This mechanism explains why a 0.2% porosity increase yields a 3.3-fold capacity enhancement. The more negative Zeta potential of AK-3 (−35.4 mV vs −27 mV for AC_o) indicates an enriched population of deprotonated hydroxyl and carboxylate groups on the carbon surface. These negatively charged sites not only attract polar FA molecules via electrostatic interactions but also facilitate the nucleophilic addition step observed in DRIFTS, where FA converts to dioxymethylene intermediates at basic oxygen sites.

Overall, in situ DRIFTS analysis demonstrates that KOH modification significantly enhances the chemical reactivity of AC_o toward FA, transforming the material from a passive adsorbent to a reactive sorbent capable of both adsorption and surface-assisted oxidation. Therefore, FA removal over AK-3 involves a synergistic mechanism combining pore-filling physisorption and surface reaction-driven chemisorption/oxidation, whereas AC_o operates predominantly through weak physical adsorption. The enhanced intensity and number of reactive surface bands for AK-3 corroborate its higher adsorption efficiency and kinetic behavior observed in other analyses [38].

3.7. Comparative analysis: FA sorption performance of AC-bases versus other sorbents

A comparative performance analysis against previously reported sorbents is essential to contextualize the efficiency and practical potential of newly developed materials. Such comparisons provide insight into whether the improvement arises from surface chemistry, porosity, or functionalization type, and help identify the most effective strategies for FA capture [45]. Comparative analysis of FA adsorption performance between the synthesized base-activated carbons (AC-bases) and other reported pristine and AC-based sorbents is presented in Table 8. Among all tested materials, the AK-3 demonstrated the highest adsorption capacity (25.52 mg g^{-1}) and a relatively high partition coefficient (PC = 0.085 mol kg^{-1} Pa^{-1}), outperforming others, including AN-2 (17.93 mg g^{-1} and 0.061 mol kg^{-1} Pa^{-1}), AC-2 (11.92 mg g^{-1} and 0.039 mol kg^{-1} Pa^{-1}), and AA-2 (14.86 mg g^{-1} and 0.048 mol kg^{-1} Pa^{-1}) (Table 8). This superior performance can be attributed to the enhanced surface basicity, increased pore accessibility, and formation of reactive oxygenated and hydroxyl functional groups introduced during KOH modification.

When compared with previously reported sorbents, such as thiourea-modified steam-activated (Table 8, entry 2 and 3), phosphoric acid activated carbons (Table 8 entry 3) (16–17 mg g^{-1}) [47], aminosilylated AC (Table 8 entry 4) (1.17 mg g^{-1}) [48], various polymer-based sorbents (Table 8 entry 5) (5.32 mg g^{-1}) [49], AC-$AgNO_3$ (Table 8 entry 6) (0.468 mg g^{-1}) [50], AC prepared from hibiscus rosa-sinensis leaves (Table 8 entry 7) (14.9 mg g^{-1}) [51], and coconut AC (Table 8 entry 8) (4.6 mg g^{-1}) [52], the AK-3 exhibited significantly higher adsorption efficiency under comparable conditions. Notably, AK-3 outperforms materials with 1.6 × larger surface areas (e.g., phosphoric-acid-activated carbon at 1659 m^2 g^{-1}, 16 mg g^{-1}) [47], proving that targeted surface-chemistry engineering surpasses

Table 8
Comparison of the FA adsorptive removal performance of AK-3 with other materials.

Order	sorbent	Modification approach	Mass of sorbent mg	Target conc. ppm	Surface area m^2/g	Adsorption capacity mg/g	PC mol kg^{-1} Pa^{-1}	references
1	Bamboo-based AC	Boric acid activation + ammonium acetate impregnation	500	0.5	240	0.075	0.05	[46]
2	steam activated	Thiourea modification	7	600	818	17	0.009	[47]
3	phosphoric acid activated carbon	Thiourea modification	7	600	1659	16	0.009	[47]
4	Aminosilylated AC	Surface functionalization	5	1	613	1.17	0.39	[48]
5	AC-P	P-modified AC	50	30	929.1	5.32	0.06	[49]
6	AC-$AgNO_3$	Surface-modified AC	100	0.5	1144	0.468	0.31	[50]
7	AC	Prepared from hibiscus rosa-sinensis leaves	300	50	12.11	14.9	0.1	[51]
8	Coconut AC	Nitric acid (HNO_3) oxidation	1500	50	1159.6	4.6	0.03	[52]
9	AC-bases	bases activation by NH_4OH	25	100	949	14.86	0.048	this work
10	AC-bases	bases activation by NaOH	25	100	968	17.93	0.061	this work
11	AC-bases	bases activation by K_2CO_3	25	100	1006	11.92	0.039	this work
12	AC-bases	bases activation by KOH	25	100	1037	25.52	0.085	this work

porosity-centric strategies. The partition coefficient of AK-3 (0.085 mol kg^{-1} Pa^{-1}) is also comparable to or higher than those of amine-functionalized materials, confirming the efficiency of base activation as a simple modification strategy [7]. Furthermore, the obtained PC values of the synthesized AC–bases (AA, AN, AC, AK) in this work (0.039–0.085 mol kg^{-1} Pa^{-1}) indicate strong FA–surface interactions comparable to or higher than those reported for amine-functionalized (thiourea-modified steam activated (0.009 mol kg^{-1} Pa^{-1}) and phosphoric acid activated carbons (0.009 mol kg^{-1} Pa^{-1})) and other ACs such as coconut AC treated with nitric acid (0.03 mol kg^{-1} Pa^{-1}). This highlights the efficiency of base activation as a simple yet powerful modification strategy for improving the adsorption potential of commercial activated carbons. Overall, the KOH-modified material (i.e., AK-3) developed in this study presents a promising, cost-effective sorbent with enhanced FA capture capacity, surpassing the majority of both pristine and AC-based materials reported in recent literature.

4. Conclusions

The synthesis of the AK-3 adsorbent via potassium hydroxide (KOH) modification of commercial activated carbon yields a material with substantially enhanced surface chemistry and superior FA adsorption performance. This single-step activation process concurrently introduces basic oxygen-containing functional groups, improves pore accessibility, and slightly increases the specific surface area (to 1037 m^2 g^{-1}). These modifications work synergistically to strengthen interactions with polar FA molecules. Consequently, AK-3 achieves the highest recorded adsorption capacity (25.52 mg g^{-1}) and partition coefficient (0.085 mol kg^{-1} Pa^{-1}) highest among the sorbents evaluated in this study, outperforming other base-activated carbons and previously reported modified activated carbon materials.

Kinetic and diffusion analyses demonstrate that FA uptake on AK-3 proceeds via a synergistic combination of physisorption within micropores and localized surface-assisted chemisorption, a process described by the Elovich model and governed by external mass transfer, intraparticle diffusion, and surface reaction steps. While low mean adsorption energy (E = 0.225 kJ mol^{-1}) confirms bulk physisorption dominance, in situ DRIFTS studies under air reveal that KOH modification converts pristine activated carbon into a chemically active sorbent. This surface-assisted oxidation pathway transforms captured FA into dioxymethylene (DOM) and surface formate ($HCOO^-$) intermediates at basic oxygen sites, yielding enhanced retention affinity alongside high micropore storage capacity. This reflects that while physical adsorption inside micropores accounts for the bulk storage capacity, KOH-induced surface oxygen functional groups supply the high retention affinity and facilitate localized chemisorption/oxidation to dioxymethylene and formate species. Complementary Zeta potential analysis supported that KOH modification imparts a more negative surface charge (−35.4 mV), providing an electrostatically favorable interface that complements micropore physisorption.

This work establishes KOH modification as a scalable strategy that achieves a 3.3-fold capacity enhancement through synergistic physisorption-chemisorption, not pore development. The mechanistic insight that surface oxygen functional groups, not porosity, govern FA uptake on commercial microporous carbon provides a design principle for next-generation sorbents: targeted surface chemistry can outperform porosity-centric strategies. AK-3 offers a cost-effective, high-performance solution for indoor formaldehyde removal, with performance competitive under humid conditions and straightforward synthesis compatible with industrial deployment.

CRediT authorship contribution statement

Kowsar Ahmadi: Writing – review & editing, Writing – original draft. **Hubdar Ali Maitlo:** Writing – review & editing. **Ki-Hyun Kim:** Writing – review & editing.

Declaration of competing interest

The authors declare the following financial interests/personal relationships which may be considered as potential competing interests:

Ki-Hyun Kim reports financial support was provided by Korea Ministry of Science and ICT. H. A. Maitlo reports financial support was provided by Korea Ministry of Science and ICT. If there are other authors, they declare that they have no known competing financial interests or personal relationships that could have appeared to influence the work reported in this paper.

Acknowledgement

This work was supported by a grant from the National Research Foundation of Korea (NRF), funded by the Ministry of Science and ICT (MSIT) of the Korean government (Grant No.2021R1A3B1068304) and by the CLEAN-AIR (Comprehensive Low Emission & Advanced Monitoring Network for Air Improvement & Renewal) R&D Program under grant number RS-2026-25504540.

This research was also supported by the Center for Polymers and Composite Materials (CPCM), Hanyang University, Korea, through the Korea Basic Science Institute (National Research Facilities and Equipment Center) grant funded by the Ministry of Education (Grant No. 2022R1A6C101A779).

Data availability

Data will be made available on request.

References

[1] Y.J. Kang, H.K. Jo, M.H. Jang, X. Ma, Y. Jeon, K. Oh, J.I. Park, Br. Rev. Formaldehyde Remov. through Act. Carbon Adsorpt., 12(10) (2022) 5025.

[2] B. Robert, G. Nallathambi, Indoor formaldehyde removal by catalytic oxidation, adsorption and nanofibrous membranes: a review, Env. Chem Lett. 19 (3) (2021) 2551–2579, https://doi.org/10.1007/s10311-020-01168-6.

[3] K. Vikrant, D.H. Lim, S.A. Younis, K.H. Kim, An efficient strategy for the enhancement of adsorptivity of microporous carbons against gaseous formaldehyde: surface modification with aminosilane adducts, Sci. Total. Environ. 743 (2020) 140761, https://doi.org/10.1016/j.scitotenv.2020.140761.

[4] W.D.P. Rengga, S. Wahyuni, A. Feinnudin, Thermodynamics of formaldehyde removal by adsorption onto nanosilver loaded bamboo-based activated carbon, Mater. Sci. Forum 890 (2017) 93–97, https://doi.org/10.4028/www.scientific.net/MSF.890.93.

[5] H. Khaleghi, H. Esmaeili, N. Jaafarzadeh, B. Ramavandi, Date seed activated carbon decorated with CaO and Fe3O4 nanoparticles as a reusable sorbent for removal of formaldehyde, Korean J. Chem. Eng. 39 (1) (2022) 146–160, https://doi.org/10.1007/s11814-021-0972-4.

[6] Ç. Murtazaoğlu, İ. Teğin, C. Saka, Facile hydrogen peroxide modification of activated carbon particles produced by potassium hydroxide activation for removal of heavy metals from aqueous solutions, Diam. Relat. Mater. 136 (2023) 110049, https://doi.org/10.1016/j.diamond.2023.110049.

[7] Y. Ahmadi, K.H. Kim, J.M. Gu, Nanodisk–like activated carbon-branched polyamine for adsorption and degradation of gaseous formaldehyde, Carbon. N. Y. 219 (2024) 118792, https://doi.org/10.1016/j.carbon.2024.118792.

[8] J.H. Kim, S.Y. Hwang, J.E. Park, G.B. Lee, H. Kim, S. Kim, B.U. Hong, Impact of the oxygen functional group of nitric acid-treated activated carbon on KOH activation reaction, Carbon Lett. 29 (3) (2019) 281–287, https://doi.org/10.1007/s42823-019-00024-0.

[9] L. Deng, J. Shi, Y. Zhao, D. Feng, W. Zhang, Y. Yu, S. Sun, Straw-based biochar prepared from multi-step KOH activation and its structure-effect relationship of CO2 capture under atmospheric/pressurized conditions via experimental analysis and MD/DFT calculations, Chem. Eng. J. 495 (2024) 153403, https://doi.org/10.1016/j.cej.2024.153403.

[10] A.A. Abdulrasheed, A.A. Jalil, S. Triwahyono, M.A.A. Zaini, Y. Gambo, M. Ibrahim, Surface modification of activated carbon for adsorption of SO2 and NOX: a review of existing and emerging technologies, Renew. Sustain. Energy Rev. 94 (2018) 1067–1085, https://doi.org/10.1016/j.rser.2018.07.011.

[11] T. Arumugham, A. Yuniarto, N. Abdullah, A. Yuzir, H. Kamyab, N.F.C. Pa, S. Rezania, M.N.M. Hatta, Preparation and characterisation of porous activated carbon using potassium hydroxide chemical activation with ultrasonic association, Biomass Convers. Biorefinery 15 (2025) 26071–26083, https://doi.org/10.1007/s13399-023-05201-w.

[12] Z. Lendzion-Bieluń, Ł. Czekajło, D. Sibera, D. Moszyński, J. Sreńscek-Nazzal, A.W. Morawski, R.J. Wrobel, B. Michalkiewicz, W. Arabczyk, U. Narkiewicz, Surface characteristics of KOH-treated commercial carbons applied for CO2 adsorption, 36 (1–2) (2018) 478–492. https://doi.org/10.1177/0263617417704527.

[13] A. Prajapati, T. Renganathan, K. Krishnaiah, Kinetic studies of CO2 capture using K2CO3/activated carbon in fluidized bed reactor, Energy Fuels 30 (12) (2016) 10758–10769, https://doi.org/10.1021/acs.energyfuels.6b01994.

[14] A. Rehman, M. Park, S.J. Park, Curr. Prog. Surf. Chem. Modif. Carbonaceous Mater., 9(2) (2019) 103.

[15] L. Deng, Y. Zhao, D. Feng, W. Zhang, Y. Yu, S. Sun, Etching physicochemical adsorption sites of biochar by steam for enhanced hydrogen storage, Chem. Eng. J. 499 (2024) 156015, https://doi.org/10.1016/j.cej.2024.156015.

[16] M.A. A.N. Mohd Faizal, A. Zaini, Dyes adsorption properties of KOH-activated resorcinol-formaldehyde carbon gels -kinetic, isotherm and dynamic studies Toxin. Rev. 41 (1) (2022) 186–197, https://doi.org/10.1080/15569543.2020.1857773.

[17] M.J. Yoo, S.H. Jo, K.H. Kim, An advanced technique for rapid and accurate monitoring of gaseous formaldehyde using large-volume injection interfaced with gas chromatograph/barrier discharge ionization detector (LVI/GC/BID), Microchem. J. 147 (2019) 806–812, https://doi.org/10.1016/j.microc.2019.03.096.

[18] L. Liu, Y. Ahmadi, K.H. Kim, D. Kukkar, J.E. Szulejko, The relative dominance of surface oxygen content over pore properties in controlling adsorption and retrograde behavior of gaseous toluene over microporous carbon, Sci. Total. Environ. 906 (2024) 167308, https://doi.org/10.1016/j.scitotenv.2023.167308.

[19] J.E. Szulejko, K.H. Kim, J. Parise, Seeking the most powerful and practical real-world sorbents for gaseous benzene as a representative volatile organic compound based on performance metrics, Sep. Purif. Technol. 212 (2019) 980–985, https://doi.org/10.1016/j.seppur.2018.11.001.

[20] L. Liu, Y. Ahmadi, K.H. Kim, D. Kukkar, J. Szulejko, Assessment of interfering/synergistic effects in the adsorption between polar and non-polar VOCs on a commercial biomass-based microporous carbon, Chemosphere 368 (2024) 143701, https://doi.org/10.1016/j.chemosphere.2024.143701.

[21] T.Y. Tran, S.A. Younis, P.M. Heynderickx, K.H. Kim, Validation of two contrasting capturing mechanisms for gaseous formaldehyde between two different types of strong metal-organic framework adsorbents, J. Hazard. Mater. 424 (Pt B) (2022) 127459, https://doi.org/10.1016/j.jhazmat.2021.127459.

[22] L. Deng, Y. Zhao, S. Sun, D. Feng, W. Zhang, Preparation of corn straw-based carbon by "carbonization-KOH activation" two-step method: gas–solid product characteristics, activation mechanism and hydrogen storage potential, Fuel 358 (2024) 130134, https://doi.org/10.1016/j.fuel.2023.130134.

[23] A. Khan, J.E. Szulejko, K.H. Kim, P. Sammadar, S.S. Lee, X. Yang, Y.S. Ok, A comparison of figure of merit (FOM) for various materials in adsorptive removal of benzene under ambient temperature and pressure, Env. Res. 168 (2019) 96–108, https://doi.org/10.1016/j.envres.2018.09.019.

[24] S. Sun, K. Vikrant, S. Verma, D.W. Boukhvalov, K.H. Kim, Diaminopropane-appended activated carbons for the adsorptive removal of gaseous formaldehyde using a portable indoor air purification unit, J. Colloid. Interface Sci. 653 (2024) 992–1005, https://doi.org/10.1016/j.jcis.2023.09.159.

[25] S. Oba, P. Ohale, Adsorptive kinetics, isotherm and thermodynamic analysis of fishpond effluent coagulation using chitin derived coagulant from waste Brachyura shell, Chem. Eng. J. Adv. 4 (2020) 100036, https://doi.org/10.1016/j.ceja.2020.100036.

[26] W.K. Kim, S.A. Younis, K.H. Kim, A strategy for the enhancement of trapping efficiency of gaseous benzene on activated carbon (AC) through modification of their surface functionalities, Environ. Pollut. 270 (2021) 116239, https://doi.org/10.1016/j.envpol.2020.116239.

[27] K. Vikrant, K.H. Kim, W. Peng, S. Ge, Y. Sik Ok, Adsorption performance of standard biochar materials against volatile organic compounds in air: a case study using benzene and methyl ethyl ketone, Chem. Eng. J. 387 (2020) 123943, https://doi.org/10.1016/j.cej.2019.123943.

[28] A. Ranjbari, A.P. Anbari, M. Kashif, K.K. Adhikary, K.H. Kim, P.M.J.C.E.J. Heynderickx, adsorpt./photocatalytic degrad. kinet. oxyg. vacancy-enriched ZnO relat. surf. funct. groups cationic/anionic dyes, 505 (2025) 159526.

[29] A. Mirghani, K. Oyedotun, O. Olaniyan, B. Mahmoud, N. Sylla, N. Manyala, Electrochemical analysis of Na–Ni bimetallic phosphate electrodes for supercapacitor applications, RSC. Adv. 9 (2019) 25012–25021, https://doi.org/10.1039/C9RA04487F.

[30] X. Wang, D. Kukkar, S.A. Younis, K. Vikrant, Y. Ahmadi, D. Boukhvalov, K.H. Kim, The co-adsorption potential of metal–organic framework/activated carbon composites against both polar and non-polar volatile organic compounds in air, Sep. Purif. Technol. 306 (2023) 122594, https://doi.org/10.1016/j.seppur.2022.122594.

[31] J. Mallouhi, M. Varga, E. Sikora, K. Gráczer, O. Bánhidi, S. Gaspard, F. Goudou, B. Viskolcz, E. Szőri-Dorogházi, B. Fiser, Activated carbon and biochar derived from Sargassum sp. Applied in polyurethane-based materials development, Polym. (Basel) 16 (2024) 2914, https://doi.org/10.3390/polym16202914.

[32] H.A. Maitlo, K.H. Kim, A. Khan, J.E. Szulejko, J.C. Kim, H.N. Song, W.S. Ahn, Competitive adsorption of gaseous aromatic hydrocarbons in a binary mixture on nanoporous covalent organic polymers at various partial pressures, Env. Res. 173 (2019) 1–11, https://doi.org/10.1016/j.envres.2019.03.028.

[33] S. Sun, S. Verma, B. Anand, S.A. Younis, D.W. Boukhvalov, K.H. Kim, Adsorption dynamics of gaseous toluene with and without formaldehyde and water vapors on composites of UiO-66-NH2 and microporous carbon, Chem. Eng. J. 498 (2024) 155605, https://doi.org/10.1016/j.cej.2024.155605.

[34] M. Yu, B. Liu, Y. Ahmadi, K.H. Kim, Practical strategies to address the moisture barriers in the adsorption of aromatic volatile organic compounds in air, Mater. Today 80 (2024) 549–564, https://doi.org/10.1016/j.mattod.2024.08.022.

[35] Y. An, X. Lv, W. Jiang, L. Wang, Y. Shi, X. Hang, H. Pang, The stability of MOFs in aqueous solutions—research progress and prospects, Green Chem. Eng. 5 (2) (2024) 187–204, https://doi.org/10.1016/j.gce.2023.07.004.

[36] W.K. Kim, S. Verma, Y. Ahmadi, M.S. Cho, K.H. Kim, The effects of metal-oxide content in MnO_2-activated carbon composites on reactive adsorption and catalytic oxidation of formaldehyde and toluene in air, Sci. Total. Environ. 926 (2024) 172137, https://doi.org/10.1016/j.scitotenv.2024.172137.

[37] Y. Hua, S. Verma, S.A. Younis, P.M. Heynderickx, K.H. Kim, Effects of gas phase composition on competitive adsorption properties of formaldehyde on titanium dioxide-supported platinum in single and mixture compositions, Sci. Total. Environ. 892 (2023) 163924, https://doi.org/10.1016/j.scitotenv.2023.163924.

[38] Y. Sun, M. Yu, S.A. Younis, K. Vellingiri, J. Szulejko, K.H. Kim, Unlocking the full adsorption potential of microporous carbon for formaldehyde in complex air mixtures, Sep. Purif. Technol. 377 (2025) 134476, https://doi.org/10.1016/j.seppur.2025.134476.

[39] T.T. Yen, K. Vikrant, J.E. Szulejko, K.H. Kim, Uncharacteristic adsorption breakthrough behavior of a core–Shell copper hydroxysulfate metal–organic framework against gaseous formaldehyde, Adv. Funct. Mater. 34 (13) (2024) 2312022, https://doi.org/10.1002/adfm.202312022.

[40] W.K. Kim, K. Vikrant, S.A. Younis, K.H. Kim, P.M. Heynderickx, Metal oxide/activated carbon composites for the reactive adsorption and catalytic oxidation of formaldehyde and toluene in air, J. Clean. Prod. 387 (2023) 135925, https://doi.org/10.1016/j.jclepro.2023.135925.

[41] H. Li, L. Cui, Y. Lu, Y. Huang, J. Cao, D. Park, S.C. Lee, W. Ho, In situ intermediates determination and cytotoxicological assessment in catalytic oxidation of formaldehyde: implications for catalyst design and selectivity enhancement under ambient conditions, Env. Sci. Technol. 53 (9) (2019) 5230–5240, https://doi.org/10.1021/acs.est.8b06234.

[42] X. Sun, J. Lin, H. Guan, L. Li, L. Sun, Y. Wang, S. Miao, Y. Su, X. Wang, Complete oxidation of formaldehyde over TiO_2 supported subnanometer Rh catalyst at ambient temperature, Appl. Catal. B: Environ. 226 (2018) 575–584, https://doi.org/10.1016/j.apcatb.2018.01.011.

[43] H.A. Maitlo, S.A. Younis, K.H. Kim, W. Yue, Z. Lu, D.H. Lim, Mechanism, performance, and application of g-C_3N_5-coupled TiO_2 as an S-scheme heterojunction photocatalyst for the abatement of gaseous benzene, ACS. Appl.

Mater. Interfaces. 17 (3) (2025) 4711–4727, https://doi.org/10.1021/acsami.4c12735.
[44] S.A. Younis, H. Shin, Y. Ahmadi, K.H. Kim, J. Lee, The effects of filter coating approaches on photocatalytic abatement of formaldehyde in indoor environment using a TiO2-based air purifier system, Env. Res. 267 (2025) 120713, https://doi.org/10.1016/j.envres.2024.120713.
[45] N.E. Williams, O.A. Oba, N.P. Aydinlik, Modification, production, and methods of KOH-activated carbon, ChemBioEng Rev. 9 (2) (2022) 164–189, https://doi.org/10.1002/cben.202100030.
[46] C. Duan, M. Meng, H. Huang, H. Wang, H. Ding, Q. Zhang, Adsorptivity and kinetics for low concentration of gaseous formaldehyde on bamboo-based activated carbon loaded with ammonium acetate particles, Env. Res. 222 (2023) 115364, https://doi.org/10.1016/j.envres.2023.115364.
[47] N. Unglaube, M. Florent, T. Otto, M. Stötzer, J. Grothe, S. Kaskel, T.J. Bandosz, Doping of porous carbons with sulfur and nitrogen markedly enhances their surface activity for formaldehyde removal, J. Colloid. Interface Sci. 653 (2024) 594–605, https://doi.org/10.1016/j.jcis.2023.09.099.
[48] K. Vikrant, D.H. Lim, S.A. Younis, K.H. Kim, An efficient strategy for the enhancement of adsorptivity of microporous carbons against gaseous formaldehyde: surface modification with aminosilane adducts, Sci Total Env. 743 (2020) 140761, https://doi.org/10.1016/j.scitotenv.2020.140761.
[49] C. Su, K. Liu, J. Zhu, H. Chen, H. Li, Z. Zeng, L. Li, Adsorption effect of nitrogen, sulfur or phosphorus surface functional group on formaldehyde at ambient temperature: experiments associated with calculations, Chem. Eng. J. 393 (2020) 124729, https://doi.org/10.1016/j.cej.2020.124729.
[50] S.M. Chang, S.C. Hu, A. Shiue, P.Y. Lee, G. Leggett, Adsorption of silver nanoparticles modified activated carbon filter media for indoor formaldehyde removal, Chem. Phys. Lett. 757 (2020) 137864, https://doi.org/10.1016/j.cplett.2020.137864.
[51] M. Zahed, D. Jafari, M. Esfandyari, Adsorption of formaldehyde from aqueous solution using activated carbon prepared from Hibiscus rosa-sinensis, Int J Env. Anal Chem 102 (13) (2022) 2979–3001, https://doi.org/10.1080/03067319.2020.1762872.
[52] X. Lu, J. Jiang, K. Sun, X. Xie, Y. Hu, Surface modification, characterization and adsorptive properties of a coconut activated carbon, Appl. Surf. Sci. 258 (20) (2012) 8247–8252, https://doi.org/10.1016/j.apsusc.2012.05.029.